APPLICATIONS OF COMPUTER VISION: SKYLINE EXTRACTION AND CONGRESSIONAL DISTRICTING

Ph.D. Thesis

Balázs Nagy

Doctoral School of Economics, Business and Informatics

Supervisor: Attila Tasnádi, D.Sc.

Department of Mathematics

Institute of Mathematics and Statistical Modelling

Corvinus University of Budapest

Budapest, 2020

Acknowledgements

Throughout the writing of this thesis, I have received a great deal of support and assistance.

I would like to thank my supervisor, Attila Tasnádi, for his dedicated support and guidance. He has continuously provided encouragement and always been supportive and enthusiastic from my undergraduate studies to the doctoral thesis. I have also learned a lot from István Deák about the practical aspects of research.

I would like to express my deepest gratitude to my colleagues, friends, and family. I cannot possibly thank my parents, my sister, and my brother enough for their support. Finally, I am deeply thankful to my wife.

Contents

List of Tables

List of Figures

List of Abbreviations

AR Augmented Reality 2, 8–13, 25, 26

DEM Digital Elevation Model 8–11, 13–15, 20, 22, 23, 63

DMC Digital Magnetic Compass 8, 9, 23, 24

EXIF Exchangeable Image File Format 22

FoV Field of View 12

GIS Geographic Information System 25

GNSS Global Navigation Satellite System 9, 13, 14, 22, 26

HFoV Horizontal Field of View 18, 19, 22

IR Infrared 13

LSI Lee-Sallee Index 49, 55, 57, 59

PPT Polsby-Popper Test 49, 55, 57, 59

RT Reock Test 49, 55, 57, 59

UAV Unmanned Aerial Vehicle 11, 13

VR Virtual Reality 10

Chapter 1

Introduction

Computer vision is an interdisciplinary field of science that tries to imitate the ability of humans how they detect and interpret visual data from the environment. According to a story, computer vision started as a student summer project at MIT in 1966. Marvin Minsky asked his undergraduate student Gerald Jay Sussman to link a computer to a camera to describe what it saw. However, this problem is effortlessly done by humans, it proved to be more complicated for computers endowed with algorithms. As Szeliski noted in 2011 [67], despite all of the advances, the aim for a computer to interpret an image at the same level as a two-year-old is a dream. Nevertheless, this discipline has developed tremendously in the last years. Nowadays, computer vision is applied in many areas, for instance, robotics, industrial automation, traffic control, navigation, medical imaging, and surveillance.

Interestingly, techniques that are developed in computer vision could be applied in social sciences as well. For example, the shape of electoral districts might be the subject of visual analysis. Drawing new electoral district boundaries or, in other words redistricting is always a controversial process since it may favor a specific party in an electoral system. Unfortunately, gerrymandering is a commonly used practice of political manipulation that dates back to 1812 when Elbridge Gerry, the governor

of Massachusetts, approved a redrawing plan of electoral districts that contained a district that reminded journalists of a salamander. This story also explains the origin of this term. Nowadays, gerrymandering is still a hot issue in the United States, where redistricting is often carried out to resolve geographic malapportionment caused by demographic changes. In fact, only a few states have an independent body in charge of this process because state legislatures usually have primary control over redistricting in their state.

Intending to connect the two seemingly distant fields, in both cases, we try to imitate humans as they percept and interpret the environment. On the one hand, matching the visible paramount peaks and landmarks around us with a large-scale map is a traditional way of orientation in mountainous terrain. On the other hand, the visual inspection of the compactness of a congressional district by an outline map is a natural way to look for political manipulation.

Our first goal is to develop an algorithm for skyline extraction, calculating the azimuth in mountainous terrain, and verify the method in a relevant environment. Our next aim is to prove that optimal partisan districting and majority securing districting are NP-complete problems, and demonstrate why finding optimal districting in real-life is challenging, as well. Finally, we intend to create a parameter-free circularity measure that can be used to detect gerrymandering and apply it to congressional districts. In this dissertation, we also study a computer vision problem and political districting problems, where Part I and Part II contain our results, respectively.

In Chapter 2, we show an effective method that can improve orientation by using skyline in an Augmented Reality (AR) mobile application. These apps, e.g., PeakVisor [62], PeakFinder [65] have a well-developed mountain identification function. They can render the digital terrain model and labels the name of peaks nearby and additional information. Some apps can also annotate uploaded pictures but the

horizontal orientation is usually imprecise, so manual fine-tuning is required for an appropriate result. It is well known that these apps have a serious problem with the accuracy of the azimuth angle provided by the sensors of the device. The fusion of the digital magnetic compass, accelerometer, and gyroscope gives the translation and rotation of the observer in the 3D space. However, the precision is usually not appropriate since the compass is prone to interference when using it near metal objects or electric currents. With the camera and a digital elevation model, a calibration can be carried out to determine the correct orientation angles. Skyline extraction is a challenging task because various visibility and weather conditions might occur. We propose an effective method to adjust the azimuth by skyline extraction that does not require manual interaction. Chapter 2 is based on Nagy [7].

In Part II, we turn to the analysis of the political districting problems and gerrymandering, which have great importance to society.

In Chapter 3, we study the districting problem from a theoretical point of view. In the middle of the previous century, it was hoped that the problem of gerrymandering could be overcome by computer programs using only data on the geographic distribution of the voters without any statistical information on voters' preferences and thus determining an unbiased districting, see Vickery [72]. The computational difficulty of the problem was clear from the very beginning, see Nagel [47]. The first algorithm finding all districtings with equally sized, connected, and compact districts was given by Garfinkel and Nemhauser [28]. Altman [2] showed that the problems of achieving any of the three mentioned criteria are NP-hard. Moreover, he also demonstrated that maximizing the number of competitive districts is also NP-hard. We show that optimal partisan districting and majority securing districting in the plane with geographical constraints are NP-complete problems. We provide a polynomial time algorithm for determining an optimal partisan districting for a simplified version

of the problem. Besides, we give possible explanations for why finding an optimal partisan districting for real-life problems cannot be guaranteed. Chapter 3 contains our results published in Fleiner et al. [26].

In Chapter 4 demonstrates an empirical study on gerrymandering. Shape analysis has special importance in the detection of manipulated redistricting. Thus we apply image moments that are widely used in image processing and computer vision. These moments are invariant to similarity transformations and can be calculated effectively. The effort to create as compact districts as possible can naturally be expected, and it is a standard criterion, see Webster [73], Polsby and Popper [54]. Hence, measuring the circularity of districts can be a suitable tool to help detect gerrymandering. The standard meaning of circularity is the degree to which a shape differs from a circle, and it is the most important index from a practical point of view. A desirable shape circularity measure should be applicable on every planar shape, ranges from 0 to 1, and it should be invariant with respect to translations, rotations, and scaling. We introduce a novel circularity measure based on Hu moment invariants. We also analyze the shape of Arkansas, Iowa, Kansas, and Utah after redistricting through multiple US Congresses. Chapter 4 is based on Nagy and Szakál [10] and [9].

Finally, in Chapter 5, a brief conclusion summarizes the thesis and presents the contributions.

Part I

SKYLINE EXTRACTION

Chapter 2

Improving the Azimuth in Mountainous Terrian

An AR application has a serious problem with the accuracy of the azimuth provided by mobile devices. The azimuth (φ) is an angular measurement between a reference direction and true north, and a line from the observer to the point of interest, projected on the same plane. The fusion of the Digital Magnetic Compass (DMC), accelerometer, and gyroscope gives the translation and rotation of the observer in 3D space. Unfortunately, the precision is not always appropriate since DMC is prone to interference when using it near metal objects or electric currents, which causes a problem in everyday use. The silhouette of ridges separates the sky from the terrain and forms the skyline or sometimes referred to as the horizon line in a mountain scenery. This salient feature can be used for orientation in both the traditional paper map way and digitally. With the camera of the device and a Digital Elevation Model (DEM), the correct azimuth can be determined. The skyline extraction from an image is a challenging task because various visibility and weather conditions might occur. We propose an effective method to adjust the azimuth by recognizing the skyline from an image and matching it with the panoramic skyline of the DEM. This algorithm

does not require manual interaction, and it has also been validated in a real-world environment.

Computer vision algorithms aim to perceive and interpret visual data coming from the environment by describing it and reconstructing its principal properties. The typical steps of a computer vision task are image acquisition, image processing, feature extraction, and decision making. There are several fields where computer vision is applied, e.g., robotics, industrial automation, transportation, navigation, medical imaging, and surveillance. Humans interpret the environment by processing information that is contained in visible light radiated, reflected, or transmitted by the surrounding objects. Due to the larger and higher resolution mobile screens, smart devices have become suitable for navigation since they are equipped with necessary sensors, such as Global Navigation Satellite System (GNSS), DMC, accelerometer and gyroscope. The GNSS and the magnetic field of Earth give a rough estimate of the position of the observer, but the accuracy of mobile sensors is not high enough for high precision AR applications. The compass is biased by metal and electric instruments nearby, although frequent calibration, so measuring the magnetic and thus the true north is not reliable. The location of the magnetic poles does not coincide with the geographic poles. Moreover, the magnetic poles are wandering around. So, the magnetic north should be corrected using a declination angle to obtain true north. Several studies, for example Blum et al. [13], Höltz et al. [31] have examined sensor reliability in real-world tests and showed the error of DMC could be as high as $10 - 30°$. The error of the gyroscope and accelerometer are also increasing with the elapsed time, and the accuracy of GNSS could be up to several meters. However, these problems are not that critical from our perspective.

Visual orientation is a three-dimensional problem of finding the orientation (pan, tilt, roll) from a geotagged photo. This task requires that the position (longitude,

latitude, elevation) of the observer is at least roughly given, the photo is taken not far from the ground, and the camera is approximately horizontal. That means the problem can be reduced to a one-dimensional instance in which the pan angle or, in other words, the azimuth needs to be determined. In this case, the camera helps to increase the precision of the other sensors by capturing visual clues whose real-world positions are known from a digital map. We propose a real-time method that extracts skyline from an image and matches it with the panoramic skyline determined from a rendered DEM. Thus, the orientation of the observer can be improved, which is critical in AR applications.

A potential application of visual orientation is mobile hiking apps that annotate mountain photos by matching images with 3D terrain models and geographic data. The ideal hiking app should have the following features: rendered 3D terrain models, highly detailed spatial data, and AR mode with automatic orientation. Popular AR apps such as PeakVisor and PeakFinder have a well-developed mountain identification function. These apps render the digital terrain model and label the name of peaks nearby with additional information. Some apps can also annotate offline geotagged images. The main problem with these programs that the horizontal orientation is usually imprecise, so a manual correction is required for an appropriate result. One of the few applications that employs sophisticated algorithms is PeakLens [53], but it focuses solely on this function. The fully panoramic 360° version of this app by La Salandra et al. [63] can be used with Virtual Reality (VR) devices too. Lütjens et al. [44] give a good example of how VR can offer intuitive 3D terrain visualization of geographical data.

Our main contribution is a novel edge-based method for automatic skyline extraction and a real-time procedure that increases the accuracy of the azimuth. This algorithm could be a module in a future AR app, as it is demonstrated in Figure 2.1.

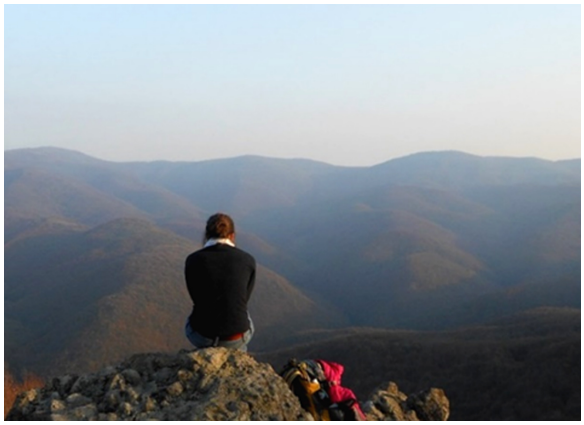

(a) Camera picture.

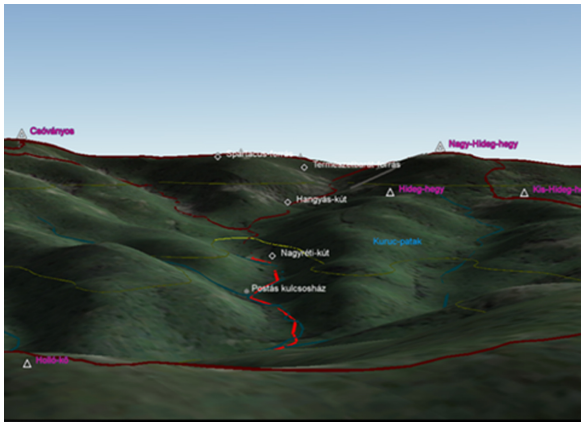

(b) DEM with geographical data.

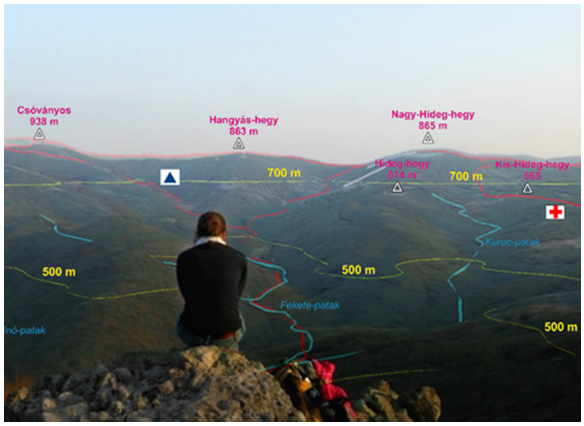

(c) AR overlay.

Figure 2.1: AR application for mountain peak identification. Source: Author.

A camera picture is shown in Figure 2.1a with a mountain ridge in the background. Figure 2.1b introduces the DEM with pertinent geographical data such as trails and peaks. The fusion of the original image and the main hiking data can be seen in Figure 2.1c.

In recent years there has been considerable interest in the challenging task of visual localization in mountainous terrain. In realistic scenarios, vegetation changes rapidly as well as lighting and weather conditions. Since the most steady and reliable feature is the contour of the mountains, people usually use the skyline and the prominent features of a landscape for orientation. This is the main idea in our approach.

Many experts have examined the so-called drop-off problem when the observer or an Unmanned Aerial Vehicle (UAV) is dropped off into an unfamiliar environment and try to locate its position. Preliminary work by Stein and Medioni [66] focused on pre-computed panoramic skyline matching with manually extracted skylines. Tzeng et al. [70] investigated a user-aided visual localization method in the desert using DEMs. Once the user marked the skyline in the query image manually, this feature was looked up in the database of panoramic skylines that had been rendered from a DEM. Camera pose and orientation estimation from an image and a DEM were studied by Naval et al. [49]. This non-real-time approach classified the sky and non-sky pixels by a previously trained neural network. Peaks and peak-like protrusions were used as feature points in the matching phase, where pre-calculated synthetic skylines were stored in a database which is not favorable in a real-time AR app due to the computation and storage needs.

Fedorov et al. [24] proposed a framework for an outdoor AR application for mountain peak detection called SnowWatch, and also described the data management approach of their solution. Sensor inaccuracy and position alignment were only partially discussed. In contrary to the present study, they took in input the device

orientation, as well. Eventually, they reached a slightly higher peak position error (1.32°) on their manually annotated dataset. SwissPeaks is another AR app that overlays peaks is presented by Karpischek et al. [36]. The main limitation of the app is that the correct azimuth should be set manually since visual feature extraction or matching was not implemented. Lie et al. [42] examined skyline extraction by a dynamic programming algorithm that looked for the shortest path on the edge map based on the assumption that the shortest path between image boundaries is the skyline. A similar solution was investigated by Hung et al. [33], where a support vector machine was trained for classifying skyline and non-skyline edge segments. A comparison of four autonomous skyline segmentation techniques that use machine learning was reviewed by Ahmad et al. [1]. The above-mentioned studies focused on skyline extraction only, and their outcomes are hard to compare with our results.

A non-real-time procedure for visual localization was suggested by Saurer et al. [64]. They introduced an approach for large-scale visual localization by extracting skyline from query images and using a collection of pre-generated, vector-quantized panoramic skylines that were determined at regular grid positions. For sky segmentation, they used dynamic programming, but their solution required manual interaction by the operator in case of the problematic pictures, which amounted to 40% of the samples. An early attempt was made by Behringer [12] to use computer vision methods for improving orientation precision. Due to computation complexity, this solution was tested in a non-real-time environment. Baboud et al. [5] also presented an automatic, but non-real-time solution for annotation and augmentation of mountainous photos. From geographical coordinates and camera Field of View (FoV), this system automatically determined the pose of the camera relative to the terrain model by using contours extracted from the 3D model. They used an edge-based algorithm for skyline detection and proposed a metric for fine-matching based on the feasible

topology of silhouette-maps. However, their algorithm was well-developed, but it is not suitable for AR applications. An unsupervised method for peak identification in geotagged photos is examined by Fedorov et al. [25]. They extracted the panoramic skyline by edge detection from the rendered DEM, but they did not address exactly how to obtain the skyline from an image.

It is worth to note that Infrared (IR) cameras were also put in an application for localization in a mountain area by Woo et al. [74]. They designed a procedure for UAV navigation based on peak extraction. Special sensors that are sensitive in the IR range could work better under lousy weather or weak light conditions. Unfortunately, a real-world test was not presented in their study.

Visual localization in an urban environment is a related problem. Several studies have been carried out on visual-aided localization and navigation in cities where the sky region is more homogeneous than other parts of the image. For instance, Ramalingam et al. [57] employed skyline, and 3D city models for geolocalization in GNSS challenged urban canyons. Zhu et al. [76] matched the panoramic skyline extracted from a 3D city model with a partial skyline form an image.

This chapter is organized as follows: Section 2.1 describes the proposed method that has three main phases:

1. panoramic skyline determination from DEM,
2. skyline extraction from the image,
3. matching the two skylines.

Section 2.2 presents the experimental results and the field test. Finally, conclusions and outlook are drawn in Section 2.3.

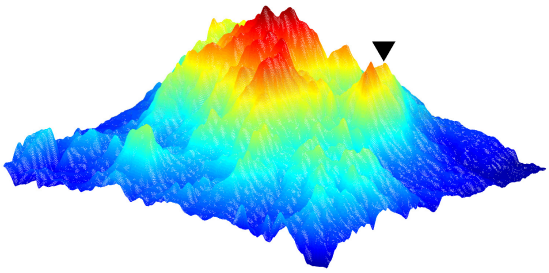

(a) Position of the observer in DEM.

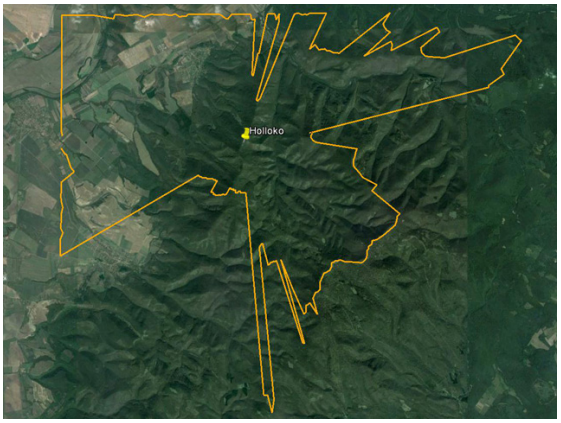

(b) Panoramic skyline on a satellite image.

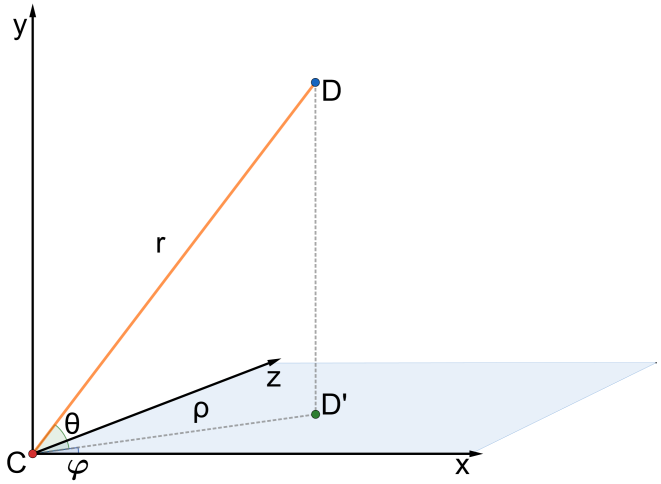

(c) Coordinate transformation.

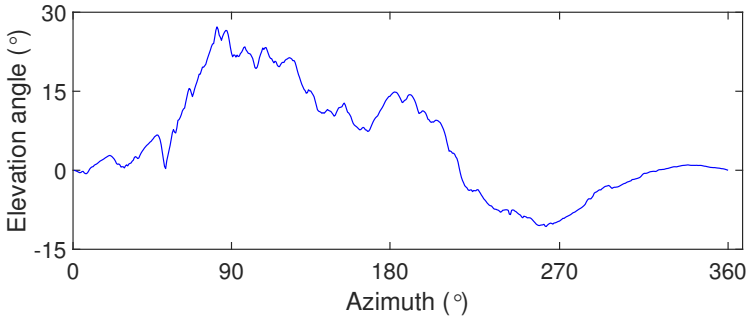

(d) Panoramic skyline vector.

Figure 2.2: The determination of the panoramic skyline. Source: Author.

2.1 Method

We propose a method that consists of three main phases. Firstly, we determine the panoramic skyline from the DEM by a geometric transformation based on the idea that Zhu et al. [76] suggested. After that, we extract the skyline from the image by a novel edge-based algorithm that uses connected component labeling. Finally, for the matching phase, we seek the largest correlation between the two skyline vectors. C++ and OpenSceneGraph were used for panoramic skyline determination. The image processing task and matching were carried out by MATLAB (Image Processing Toolbox). The georeferencing for the field tests was made with Google Earth Pro and QGIS.

2.1.1 Panoramic Skyline Determination

Panoramic skyline is a vector obtained from the 3D model of the terrain. We used publicly available DEMs: SRTM [23] and ASTER [48], sampled at a spatial resolution between 30m and 90m. Depending on the distance of the viewpoint from the target and characteristic of the terrain in the corresponding geographical area that could be a bit coarse, but in most cases, this resolution was enough. Figure 2.2 demonstrates this phase. Figure 2.2a shows a rendered DEM, where the black triangle is the position of the camera, which was determined by the GNSS sensor of the device. The 360° panoramic skyline was calculated from this point by a coordinate transformation, as Figure 2.2c shows, where

- $C(X_0, Y_0, Z_0)$ is the position of the camera,
- $D(X, Y, Z)$ is an arbitrary point of the DEM,
- $D'(x', y', z')$ is the projection of point D. [1]

[1] $y' = Y_0$

Hereby, each point can be described by the azimuth angle:

$$\varphi = \begin{cases} 0 & \text{if } X = X_0 \text{ and } Z = Z_0 \\ \arcsin\left(\frac{z'-Z_0}{\rho}\right) & \text{if } X \geq X_0 \\ -\arcsin\left(\frac{z'-Z_0}{\rho}\right) + \pi & \text{if } X < X_0 \end{cases}$$

and the elevation angle:

$$\theta = \arcsin\left(\frac{Y - y'}{r}\right)$$

where

$$\rho = \sqrt{(x' - X_0)^2 + (z' - Z_0)^2}$$

is the distance between C and D' and

$$r = \sqrt{(X - X_0)^2 + (Y - Y_0)^2 + (Z - Z_0)^2}$$

is the distance between C and D. A 3D to 2D transformation was applied since the height information, or the radial distance is no longer required. Azimuth angle ϕ and the elevation angle θ describe any point D in the DEM. Finally, the largest θ value determines the demanded point of the skyline for each φ. Figure 2.2b illustrates the panoramic skyline projected on a satellite image. The sharp edges on the left corner indicate the border of the DEM because the skyline was calculated only at a reasonable distance. Figure 2.2d shows the output, i.e., the panoramic skyline vector that will be used in the matching phase.

2.1.2 Skyline Extraction

The skyline sharply demarcates terrain from the sky on a landscape photo. Our novel and automatic skyline extraction method is presented in the following. The main idea is based on the experience that large and wide connected components in the upper region of the image usually belong to the skyline.

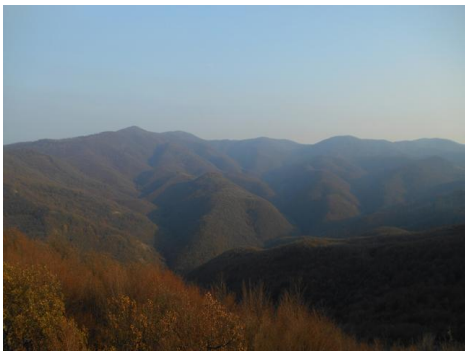

(a) Original image.

(b) Morphological operations.

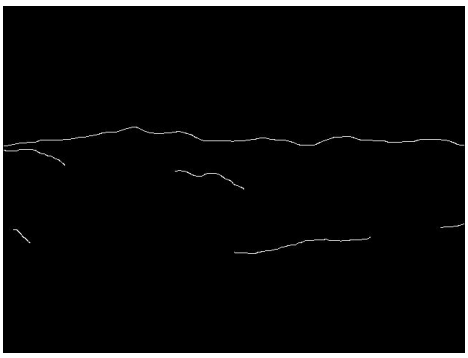

(c) Edge map.

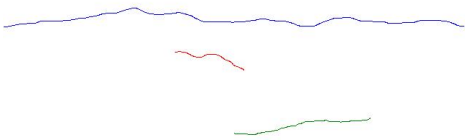

(d) Skyline candidates.

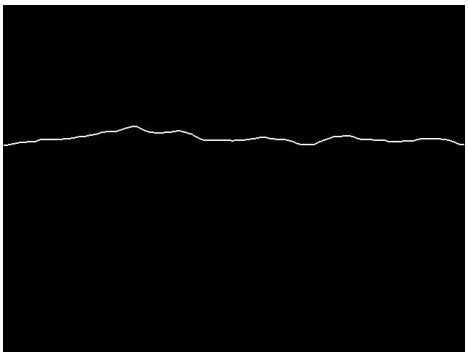

(e) Top-down search.

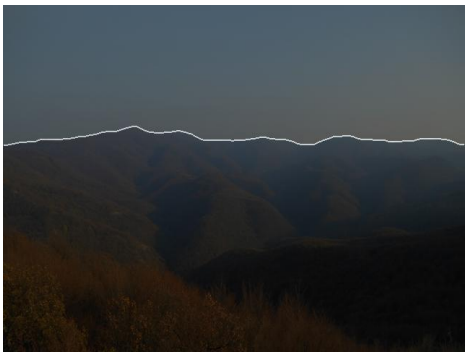

(f) The extracted skyline.

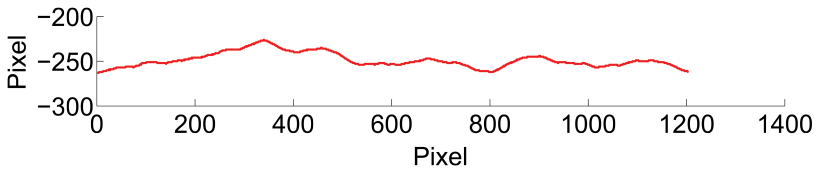

(g) The skyline vector.

Figure 2.3: The extraction of the skyline. Source: Author.

A well-known algorithm for connected components labeling was used for finding blobs in a binary image. It is an algorithmic application of graph theory, where connected components are labeled uniquely. Figure 2.4a shows an input binary image with disjoint edge segments that are colored to different shades of gray in the output, as Figure 2.4b shows. A flood-fill algorithm was applied for finding 8-connected components (8-connected neighborhood), where pixels touch one of their edges or corners, i.e., they are connected horizontally, vertically, or diagonally. A detailed review of connected components labeling is found in He et al. [29]. It is not necessary to detect the whole skyline since, in most cases, recognizing only an essential part of it is enough for matching. On the other hand, it is crucial to extract a piece from the real skyline and not a false edge. Statistically speaking, the False Acceptance Rate (Type II error) should be as low as possible, while the False Rejection Rate (Type I error) is not that critical.

In the preprocessing phase, morphological operations were carried out to enhance the grayscale image and remove noise. Morphological closing (dilation and erosion) eliminate small holes, while morphological opening (erosion and dilation) removes small objects from the foreground that are smaller than the structuring element. A disk-shaped structuring element was used either for closing and opening but with a different radius (5 and 10 pixels). Details on morphology can be found in, e.g., Szeliski [67].

The following algorithm selects the skyline from skyline candidates in multiple steps. The candidates were sorted by the function

$$S(C) = \mu(C) + 2\rho(C),$$

where C is a skyline candidate, μ measures the number of pixels in the candidate and ρ is the span of the candidate, i.e., the difference between the rightmost and the leftmost pixel coordinates in the image space.

This function takes into account the size and the span of C with double weight, which is proved to be efficient according to our observations. Therefore, larger and broader skyline candidates are preferred.

The main steps are listed below and also shown in Figure 2.3.

1. Preprocessing

   (a) The first step is to resize the original image to 640×480 pixels and adjust the contrast. (Figure 2.3a)

   (b) The sky is in the sharpest contrast to the terrain in the blue color channel in RGB color space. Thus we use the blue channel as a grayscale picture.

   (c) Morphological closing and opening operations are applied for smoothing the outlines, reducing noise, and thereby ignoring the useless details, e.g., edges of tree branches or rocks. (Figure 2.3b)

   (d) The edge detection is carried out by the Canny edge detector [15] results in a bitmap that contains the most distinctive edges on the image. (Figure 2.3c)

2. Connected components labeling detects the connected pixels on the edge map determining the skyline candidates. The top three skyline candidates are chosen by the function S. (Figure 2.3d)

3. A top-down search selects the first edge pixels from the most probable candidates in each column because the skyline should be on the upper region of the image. (Figure 2.3e)

4. In case of low resolution, the top-down search might make a one-pixel gap in the skyline. A so-called bridge operation repairs this problem by filling the holes.

5. The second connected component analysis eliminates the left-over pieces from the edge map and selects the largest one as the presumed skyline. (Figure 2.3f)

6. Finally, the skyline is vectorized for the matching phase. (Figure 2.3g)

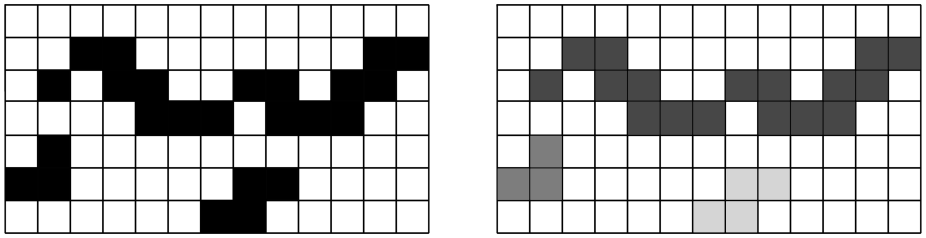

(a) Binary image. **(b)** Three disjoint components.

Figure 2.4: Connected components labeling. Source: Author.

2.1.3 Skyline Matching

The last phase of the proposed method is matching the panoramic skyline and the recognized fragment of the skyline from the image. We look for the point from where the skyline vectors interlock, i.e., the image skyline fits into the panoramic skyline. The φ could be obtained from here. It is worth noting that for the proper comparison, the Horizontal Field of View (HFoV) of the camera and the panoramic skyline [2] need to be synchronized via the sampling rate of the two signals. For the sake of simplicity, the first index of the panoramic skyline vector corresponds to 0° (true north) as a reference point. In the case of partially extracted image skyline, the gap also should be considered in accordance with HFoV, so the total width of the skyline is estimated.

After that, normalized cross-correlation ($a \star b$) is used, which is commonly used in signal processing as a measure of similarity between a vector a (panoramic skyline) and shifted (lagged) copies of a vector b (extracted skyline) as a function of the lag k.

[2] The HFOV of the panoramic skyline is 360°.

After calculating the cross-correlation between the two vectors, the maximum of the cross-correlation function indicates the point K where the signals are best aligned:

$$K = \underset{0° \leq k < 360°}{\operatorname{argmax}} ((a \star b)(k)).$$

From K the azimuth φ can be determined, and the estimated horizontal orientation can be acquired. As it was mentioned above, the camera is supposed to be approximately horizontal when the picture was taken, though the skyline could be slightly slanted. The cross-correlation is not sensitive to such inaccuracies, so this approach is suitable for matching the skylines. An example of matching the panoramic skyline (blue) with the extracted skyline (red) is presented in Figure 2.5.

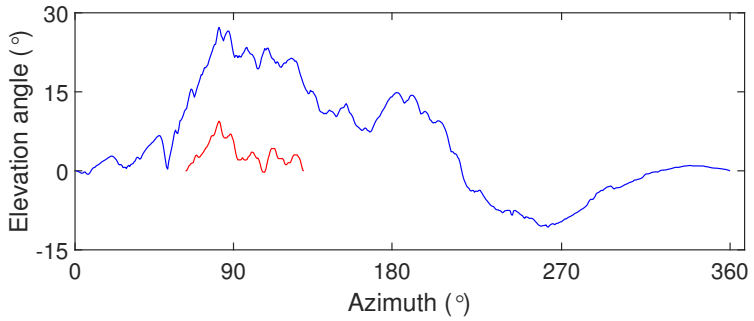

Figure 2.5: Matching of the panoramic skyline with the extracted skyline. Source: Author.

2.2 Experimental Results

Our goal was to develop a procedure that can determine the exact orientation of the observer in a mountainous environment by a geotagged camera picture and a DEM. The main contribution of this paper was an edge-based skyline extraction method. Thus the first part of this section demonstrates the results on sample images. The second part is about calculating the azimuth (φ) and comparing the results with

the ground truth azimuth ($\hat{\varphi}$) determined by traditional cartographic methods using reference objects.

2.2.1 Skyline Extraction

Skyline extraction is a crucial task in this method. The whole pattern is not necessarily needed for the correct alignment because, in most cases, only a characteristic part of the skyline is enough for matching. The algorithm was tested on a sample set that contains mountain photos from various locations, seasons, under different weather and light conditions. The goal was to extract the skyline as precisely as possible, therefore to somehow evaluate the results, we also classified the outputs. The pictures were made by the author, or they were downloaded from Flickr under the appropriate Creative Commons license. The collection consists of 150 images with 640×480 pixels resolutions and 24-bit color depth. Experiments showed that this resolution provides good results considering computation performance, as well. Figure 2.6 illustrates the automatic skyline extraction steps on four different examples: (a) shows a craggy mountain ridge with clouds and rocks that could have misled an edge detector; in (b) the snowy hills blend into the cloudy sky mountain which makes skyline detection difficult; (c) is taken from behind a blurry window, where raindrops and occluding tree branches could have impeded the operation of an algorithm; (d) demonstrates a hard contrast image with a clear skyline, where clouds might have induced false skyline edges. The detailed description of the steps can be found in Section 2.1. For more examples, see Appendix A.

The outputs were classified into four classes according to the quality (%) of the result. The evaluation was done manually because an objective measure is hard to create.

- Perfect: the whole skyline $[95 - 100\%]$ is detected, no interfering fragments

Class	Rate
Perfect	56.67%
Good	32.67%
Poor	8.00%
Bad	2.67%

Table 2.1: Results of automatic skyline extraction method.

found.

- Good: the better part of the skyline $[50 - 95\%)$ is detected, false pixels do not affect the analyses.
- Poor: only a small part of the skyline $[5 - 50\%)$ is detected, false pixels might affect the analyses.
- Bad: skyline cannot be found or the detected edges do not belong to the skyline $[0 - 5\%)$.

Table 2.1 shows that the extracted skylines are assigned to Perfect or Good classes in more than 89% of the samples. In these cases, the extracted features can be used for matching in the next phase. It is noteworthy that the rate of *poor* is 8% and *bad* outcomes is less than 3%. When the algorithm fails, the difficulties usually arise from occlusion, foggy weather, or low light conditions. In some cases, when the picture is hard contrast with plenty of edges, e.g., deceptive clouds, or rocks, the largest connected component did not necessarily belong to the skyline, and it is difficult to find the horizon line even with the naked eye.

2.2.2 Field Tests

Unfortunately, it was not possible to compare the results directly with those obtained by other methods discussed above, due to the different problems they addressed. Therefore, we made field tests to measure the performance of our algorithm. The experiments aimed to determine the orientation using only a geotagged photo and the DEM. A Microsoft Surface 3 tablet was employed, which has an in-built GNSS sensor and an 8MP camera sensor with 53.5° HFoV. Various pictures were taken in the mountains with clearly identifiable targets such as church or transmission towers and aligned them into the center of the image with the help of an overlying grid. The Exchangeable Image File Format (EXIF) data contains the position, so a recognizable target concerning the viewpoint could be manually referred, so $\hat{\varphi}$ was determined for the 10 sample images. The low sample size is due to the difficult task of locating test points and the lack of a publicly available image data set with georeferenced objects.

Figure 2.7 shows example images with the extracted skyline (white), the panoramic skyline (orange), and the reference object (yellow cross) that was aligned to the center of the picture. Table 2.2 presents the experimental results of the field tests. Only Good and Perfect skylines were accepted for the tests, and the correlation is almost 95% on average. The mean of absolute differences between $\hat{\varphi}$ and φ is 1.04°, which is auspicious.

As it was mentioned above, the error of DMC could be $10 - 30°$. Measuring the inaccuracy of the compass sensor is beyond the scope of this study. Nevertheless, this problem was experienced during field tests. The benefit of the proposed algorithm is the precise orientation obtained by the camera picture and a DEM. The field tests demonstrated that it could be achieved with this method. The average 1.04° error is mainly caused by the coarse resolution of DEMs and the vegetation. Thus, the results might be enhanced with a higher resolution DEM.

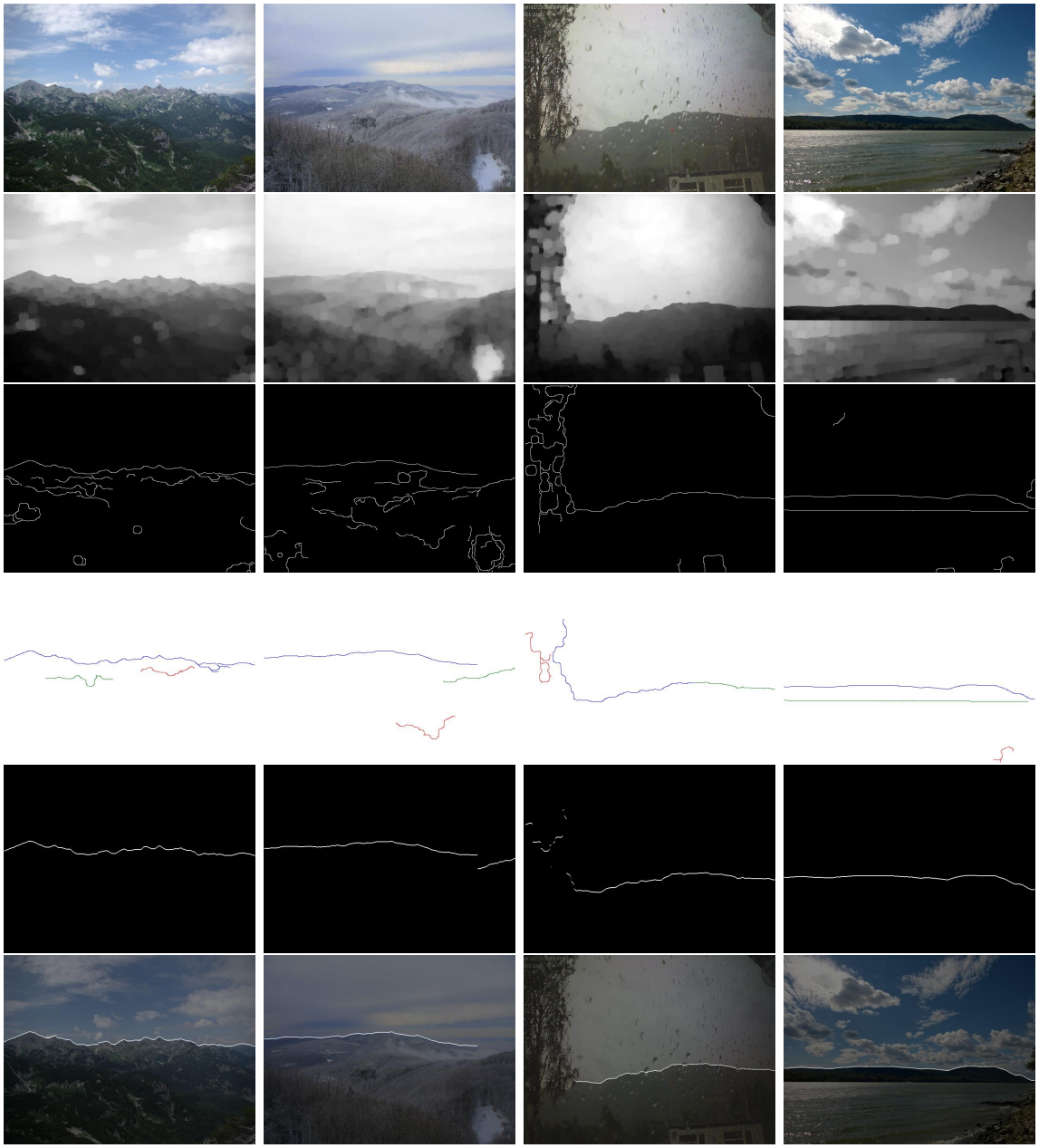

(a) Example 1. **(b)** Example 2. **(c)** Example 3. **(d)** Example 4.

Figure 2.6: Some examples of automatic skyline extraction. Source: Author.

2.3 Concluding Remarks

This chapter proposed an automatic method for improving the azimuth measured by the unreliable DMC sensor in mountainous terrain. The aim was to develop an algo-

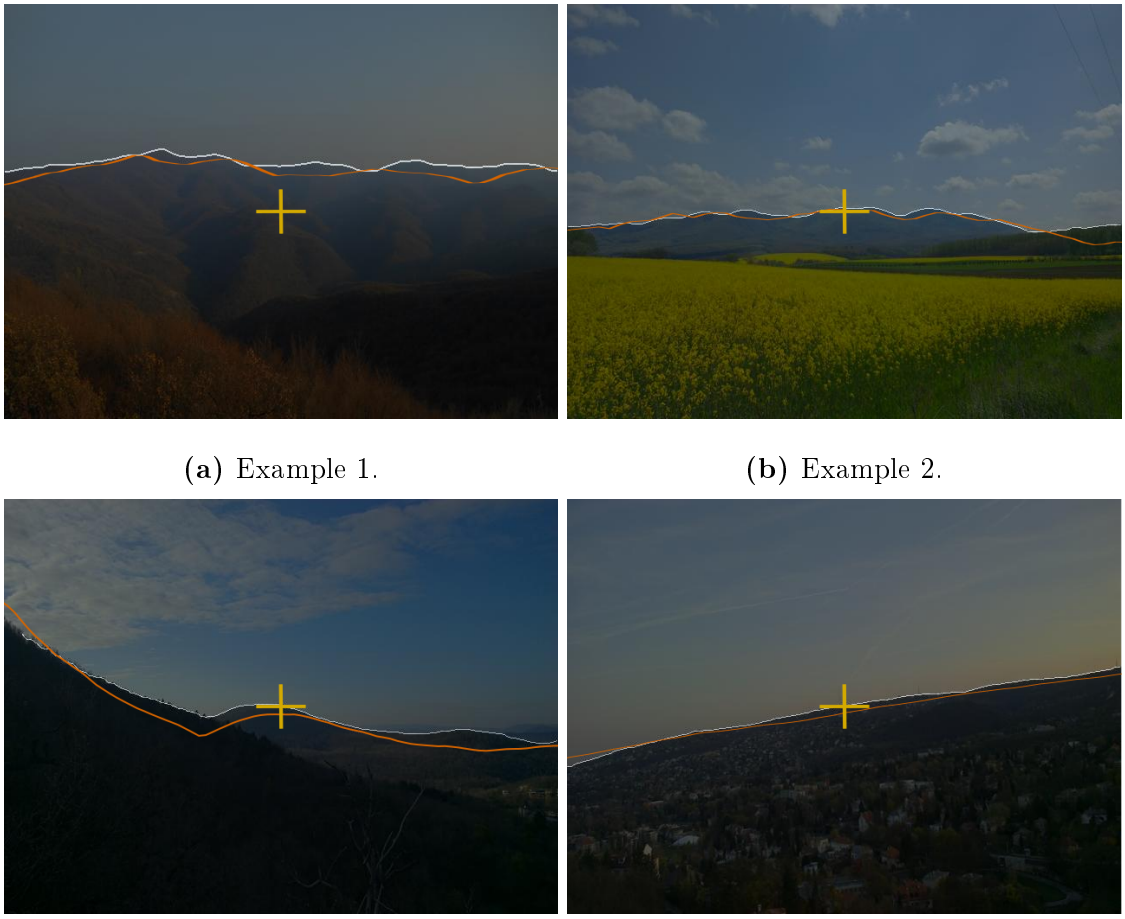

(a) Example 1. **(b)** Example 2.

(c) Example 3. **(d)** Example 4.

Figure 2.7: Field test images with the extracted skyline, the panoramic skyline, and the reference object. Source: Author.

rithm for an outdoor AR app that overlays useful information about the environment from a Geographic Information System (GIS) such as peak names, heights, or distances. The main contribution of this work is the robust skyline extraction procedure that employed connected components labeling. The skyline was extracted successfully in more than 89% of the sample set. Furthermore, field tests were also carried out to verify the skyline matching, as well. The deviation of the azimuth provided by the algorithm and the ground truth azimuth is 1.04° on average. Performance issues were beyond the scope of this study, but the algorithm is time and storage ef-

Image	Viewpoint			Target			Results			
ID	Lat (°N)	Lon (°E)	Height (m)	Lat (°N)	Lon (°E)	Height (m)	Corr.	φ (°)	$\hat{\varphi}$ (°)	$\hat{\varphi} - \varphi$ (°)
FT01	47.51552	18.96866	330	47.55016	19.00178	436	0.92	31.58	32.60	**1.02**
FT02	47.51552	18.96866	330	47.53371	18.95588	429	0.96	334.62	334.61	**-0.01**
FT03	47.55555	18.99883	483	47.51827	18.95922	508	0.95	214.83	215.61	**0.78**
FT04	47.53154	18.98611	219	47.49178	18.97895	458	0.99	185.89	186.95	**1.06**
FT05	47.99865	18.86120	188	47.99564	18.86353	195	0.92	151.35	152.47	**1.12**
FT06	47.99948	18.86173	201	47.99564	18.86353	195	0.98	161.22	162.92	**1.70**
FT07	47.51827	18.95922	508	47.55016	19.00178	436	0.97	44.12	41.85	**-2.27**
FT08	47.98355	18.80440	124	47.95780	18.87714	723	0.88	118.98	118.58	**-0.40**
FT09	47.99865	18.86120	188	47.99564	18.86353	195	0.94	151.52	152.47	**0.95**
FT10	47.99948	18.86173	201	47.99564	18.86353	195	0.98	161.81	162.92	**1.11**

Table 2.2: Experimental results of the field tests.

ficient. The results are promising, and they showed that the proposed method could be applied as an autonomous, highly accurate orientation module in a real-time AR application. With suitable data and some adaptation, the system might be used for visual localization in GNSS challenged urban environment.

Part II

CONGRESSIONAL DISTRICTING

Chapter 3

Optimal Partisan Districting on Planar Geographies

In this chapter, we examine districting in a particular framework from a theoretical point of view. We show that optimal partisan districting and majority securing districting in the plane with geographical constraints are NP-complete problems. Furthermore, we provide a polynomial time algorithm for determining an optimal partisan districting for a simplified version of the problem. Besides, we give possible explanations for why finding an optimal partisan districting for real-life problems cannot be guaranteed.

In electoral systems with single-member districts or even with at least two multi-member districts, redistricting has to be carried out to resolve geographic malapportionment caused by migration and different district population growth rates. An inherent difficulty associated with redistricting is that it may favor a party. The problem becomes even worse if redistricting is manipulated for an electoral advantage, which is referred to as gerrymandering.

In the middle of the previous century, it was hoped that the problem of gerrymandering could be overcome by computer programs using only data on voters' ge-

ographic distribution without any statistical information on voters' preferences and thus determining an unbiased districting, see Vickery [72]. The first algorithm finding all districtings with equally sized, connected, and compact districts was given by Garfinkel and Nemhauser [28]. Earlier Hess et al. [30] provided an algorithm striving for similar goals. However, their algorithm did not always obtain optimal solutions. The computational difficulty of the problem was clear from the very beginning. Nagel [47] documented in an early survey the computational limitations of automated redistricting by considering the available programs of his time. Altman [2] showed that the problems of achieving any of the three mentioned criteria are NP-hard. Moreover, he also demonstrated that maximizing the number of competitive districts is also NP-hard. Because of the computational difficulty of the problem there is a growing literature on new approaches to finding unbiased districtings, see, for instance, Mehrotra [46], Bozkaya et al. [14], Bacao et al. [6], Chou and Li [19], Ricca [61], Ricca et al. [60]. For recent surveys, we refer to Ricca et al. [59], Tasnádi [69], Kalcsics [35].

Though finding an equally sized districting is already computationally hard, from another point of view it is feared by the public that the continuously increasing computational power makes the problem of carrying out optimal partisan gerrymandering possible. However, the underlying difficulty of the problem does not allow us to determine an optimal partisan redistricting. Indeed, Altman and McDonald [3] provide recent evidence that current computer programs are far away from finding optimal gerrymandering.

A formal proof establishing that a simplified version of the optimal gerrymandering problem is NP-complete was given by Puppe and Tasnádi [56]. They took geographical constraints into account, but planarity was not prescribed explicitly. In recent work, Lewenberg et al. [41] also proved the NP-completeness of optimal ger-

rymandering in the plane. However, they did not demand equally or almost equally sized districts.

This chapter is organized as follows. In Section 3.1, we introduce the most important definitions. In Section 3.2, we show that winning an election, i.e., deciding the existence of a districting that guarantees a majority of a party is also NP-complete. Furthermore, for districting problems that can be simplified to a one-dimensional districting problems, we provide a polynomial time algorithm for finding the optimal partisan districting. In Section 3.3, we bring forward arguments in favor of the computational intractability of determining an optimal partisan districting for real-life problems of modest size. Finally, conclusions are drawn in Section 3.4.

3.1 The Framework

We assume that parties A and B compete in an electoral system consisting only of single member districts. A single member district is an electoral district returning only one representative to an office. In addition, voters with known party preferences are located in the plane and have to be divided into a given number of almost equally sized districts. The districting problem is defined by the following structure:

Definition 3.1.1. *A* districting problem *is given by* $\Pi = (X, N, (x_i)_{i \in N}, v, K, \mathcal{D})$, *where*

- X *is a bounded and strictly connected*[1] *subset of* $\mathbb{R}^2$,
- *the finite set of voters is denoted by* $N = \{1, \ldots, n\}$,
- *the distinct locations of voters are given by* $x_1, \ldots, x_n \in \text{int}(X)$,
- *the voters' party preferences are given* $v : N \to \{A, B\}$,

[1] We call a bounded subset A of $\mathbb{R}^2$ *strictly connected* if its boundary ∂A is a closed Jordan curve.

- *the set of district labels is denoted by* $K = \{1, \ldots, k\}$*, where* $\lfloor n/k \rfloor \geq 3$*, and*
- $\mathcal{D}$ *denotes the finite set of admissible districts consisting of bounded and strictly connected subsets of* X *and each of them containing the location of* $\lfloor n/k \rfloor$ *or* $\lceil n/k \rceil$ *voters,*[2] *and furthermore,*
- *we shall assume that based on their locations the* n *voters can be partitioned into* k *districts* $\{D_1, \ldots, D_k\} \subseteq \mathcal{D}$*.*

Observe that in defining the districting problem, we assumed that obtaining an almost equally sized districting is possible, which can be justified by the fact that finding an admissible districting for real-life problems is possible, while finding a districting satisfying additional requirements such as partisan optimality is difficult. In particular, the staff hired to produce a districting map could always construct a districting map consisting of almost equally sized districts, although other properties like partisan optimality are difficult to prove or to confute. Producing a districting with almost equally sized districts is a tractable problem if there are not too many geographical restrictions since then we can obtain a result by drawing districts from left to right and from top to bottom on a map of a state by keeping the average district size in mind. An initial step for such an algorithm would be, for instance, to order the voters increasingly according to their horizontal or vertical coordinates.

We shall mention that in reality, the basic units of a districting problem from which districts have to be created are census blocks or electoral wards rather than voters in order to simplify the problem, and at the same time to include natural municipal boundaries. In this case, voter preferences $v : N \to \{A, B\}$ have to be replaced by a function of type $v' : N' \to [0, 1]$, where N' stands for the finite set of wards, assigning to each ward a fraction of party A voters. However, our results

[2] $\lfloor x \rfloor$ stands for the largest integer not greater than $x \in \mathbb{R}$ and $\lceil x \rceil$ stands for the smallest integer not less than $x \in \mathbb{R}$.

obtained in this work can be extended to this more general setting by allowing the case of almost equally sized wards. For this, district outcomes are determined by the number of winning wards for party A, which happens to be the case, for instance, if $v'(N') = \{\alpha, 1-\alpha\}$ for a given $\alpha \in [0, 1/2)$, i.e., the fraction of party A voters in each ward equals either α or $1-\alpha$, and thus the main result of this study delivers a worst case scenario for the model with wards as elementary units. Hence, the NP-completeness results in this study imply the same NP-completeness results within a model with almost equally sized wards and districts, which come closer to the problems handled by gerrymanderers.

Turning back to our districting problem defined on the level of voters, we have to assign each voter to a district.

Definition 3.1.2. *An $f : N \to \mathcal{D}$ is a* districting *for problem Π if there exists a set of districts $D_1, \ldots, D_k \in \mathcal{D}$ such that*

- $f(N) = \{D_1, \ldots, D_k\}$,
- $\text{int}(D_i) \cap \text{int}(D_j) = \emptyset$ [3] *if $i \neq j$ and $i, j \in K$,*
- $\{x_i \mid i \in f^{-1}(D_j)\} \subset \text{int}(D_j)$ *for any $j \in K$.*

Observe that without loss of generality we do not explicitly require that a districting covers the entire country, but just the inhibited areas.

Definition 3.1.3. *Two districtings $f : N \to \mathcal{D}$ and $g : N \to \mathcal{D}$ with districts $D_1, \ldots, D_k$ and $D'_1, \ldots, D'_k$, respectively, are* equivalent *if there exists a bijection between the series of sets $\{x_i \mid i \in f^{-1}(D_1)\}, \ldots, \{x_i \mid i \in f^{-1}(D_k)\}$ and the series of sets $\{x_i \mid i \in g^{-1}(D'_1)\}, \ldots, \{x_i \mid i \in g^{-1}(D'_k)\}$ such that the respective sets are identical.*

[3] $\text{int}(A)$ stands for the interior of set A.

Clearly, by defining equivalent districtings we have defined an equivalence relation above the set of districtings for problem Π.

A districting f and voters' preferences v determine the number of districts won by parties A and B, which we denote by $F(f, v, A)$ and $F(f, v, B)$, respectively. If the two parties should receive the same number of votes in a district, its winner is determined by a predefined tie-breaking rule $\tau : \mathcal{D} \to \{A, B\}$.

Definition 3.1.4. *For a given problem* Π *and tie-breaking rule* τ *a districting* $f : N \to \mathcal{D}$ *is* optimal *for party* $I \in \{A, B\}$ *if* $F(f, v, I) \geq F(g, v, I)$ *for any districting* $g : N \to \mathcal{D}$.

Note that due to the above defined equivalence relation the set of districtings has finitely many equivalence classes, and therefore there exists at least one optimal districting for each party.

3.2 Determining an Optimal Districting

We establish that even the decision problem associated with the optimization problem of determining an optimal partisan districting, i.e., deciding for a given districting problem Π whether there exists a districting with at least m winning districts for a party, say party A, is an NP-complete problem. We call this WINNING DISTRICTS problem. In order to prove this, we shall reduce the INDEPENDENT SET problem on planar cubic[4] graphs, a proven NP-complete problem, see Garey and Johnson [27], to WINNING DISTRICTS. The INDEPENDENT SET problem asks whether a given graph G has a set of non-neighboring vertices of cardinality not less than m.

Theorem 3.2.1. *WINNING DISTRICTS is NP-complete.*

[4] A graph is cubic if the degree of each vertex equals 3.

Proof. Whether a districting possesses at least m winning districts for party A can be verified easily in polynomial time, and therefore WINNING DISTRICTS is in NP.

We establish that INDEPENDENT SET on planar cubic graphs reduces to WINNING DISTRICTS. We define the mapping that assigns to an arbitrary planar cubic graph $G = (V, E)$ a districting problem. We may assume that the graph is embedded in the plane such that all the edges are straight lines and denote the set of their midpoints by V_E. We define ε as the minimum of the distances between a point of $V \cup V_E$ and a non-incident edge. The layout of the districts and the reduction can be seen in Figure 3.1. The 3-star of a vertex $v \in V$ is the union of the three line segments between v and the midpoints of the three edges emitting from v.

Let the set of party A voters be V_E and with each party A voter $M \in V_E$ we associate two party B voters M' and M'' such that M', M and M'' lie in this order on the same straight line perpendicular to the edge of M and the distance of M' and M'' from M is between $\frac{1}{5}\varepsilon$ and $\frac{2}{5}\varepsilon$.

For each midpoint $M \in V_E$ we construct a party B winning district as the $\frac{2}{5}\varepsilon$-neighborhood of M. Since each of these districts contains two-party B voters and a party A voter, so we call them mixed districts.

We associate with each vertex $v \in V$ a party A winning district as the $\frac{1}{5}\varepsilon$-neighborhood of the 3-star of v. Observe that this district contains exactly three voters, and they are the midpoints of the edges of v thus we call it A-uniform district.

Consider the set-theoretic difference of the $\frac{2}{5}\varepsilon$-neighborhood and $\frac{1}{5}\varepsilon$-neighborhood of the 3-star of v, i.e., the subset of the plane consisting of the points having distance from the 3-star between $\frac{1}{5}\varepsilon$ and $\frac{2}{5}\varepsilon$. This set contains exactly six voters, which are the party B voters corresponding to the midpoints of the edges of v. It is straightforward to see that the bisector of any angle defined by the edges at v and the edge different from the sides of that angle divide this set in such a way that each part contains

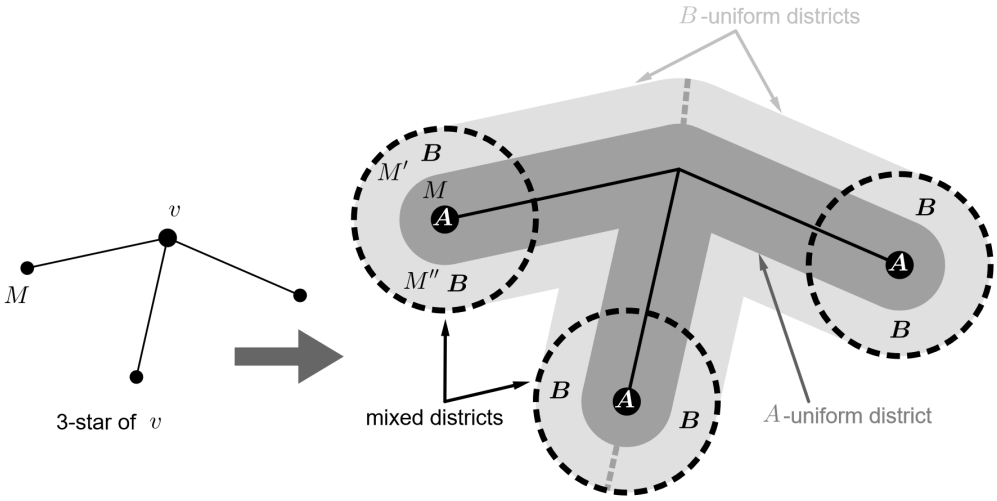

Figure 3.1: The layout of the districts. Source: Author.

three-party B voters. We call these divided parts B-uniform districts.

Now, it is enough to show that the graph G has an independent set of size m if and only if the above-defined districting problem has a districting with m party A winning districts.

The sufficient part of this claim is obvious since the party A winning districts of a districting are disjoint A-uniform districts, and they correspond to non-neighboring graph vertices.

For the necessary part, we construct for any given independent set of size m a districting having m A winning districts. Take the A-uniform and B-uniform districts corresponding to the vertices of the independent set and for the still uncovered voters, take their mixed districts. Clearly, all the voters are covered by a district, and it is not hard to see because of the choice of ε that the chosen districts are disjoint and each contains three voters.

We note that the associated districting problem described above can be determined in polynomial time. □

The following easy consequence of Theorem 3.2.1 has practical importance.

Theorem 3.2.2. *The decision problem whether a districting problem* Π *has a districting in which party* A *gains majority is NP-complete.*

Proof. Note that all districtings in the proof of Theorem 3.2.1 have $\frac{3}{2}|V|$ districts. Thus there exists a districting with at least m winning districts of party A if and only if the following districting problem extended with dummy voters and districts has a solution in which the A winning districts form a majority. Let us add $\frac{3}{2}|V|-2m+1$ extra disjoint A winning districts each containing three extra A voters if $m \leq \frac{3}{2}|V|/2$, otherwise add $2m - \frac{3}{2}|V|-1$ extra disjoint B winning districts with three extra B voters in each. □

Remark. *The notion of majority in Theorem 3.2.2 is irrelevant. The same statement can be proved by analogy for any qualified majority.*

3.2.1 A Positive Result

As we have seen in Theorem 3.2.1, finding an optimal districting is difficult. The problem becomes tractable if we replace $\mathbb{R}^2$ with $\mathbb{R}$ in Definition 3.1.1, i.e., if we restrict the two-dimensional problem to a one-dimensional one. Observe that X and the admissible districts become intervals. For the sake of simplicity, we assume that $X = [0, n]$, voter i is in the i^{th} unit interval, i.e., $x_i \in (i-1, i)$, and the admissible districts have the form of $[a, b]$ where $a, b \in \{0, 1, 2, \ldots, n\}$ and $a < b$. If n is divisible by k, the problem of finding a partisan optimal districting is trivial. Therefore, in the remainder of this subsection we assume that n is not divisible by k. Then the admissible districts may contain either $\lfloor n/k \rfloor$ or $\lceil n/k \rceil$ voters, which we will call short and long districts, respectively, and denote their lengths by s and l, respectively.

Based on the dynamic programming technique, we develop a polynomial time

algorithm that finds a so-called party A optimal districting for the one-dimensional districting problem.

For expositional reasons, we define the indicator function $w : \mathcal{D} \to \{0, 1\}$ such that $w([a, b]) = 1$, if the district $[a, b]$ is won by party A and $w([a, b]) = 0$, otherwise. We will keep a record of the variables $W_i(j)$ (for $j \in \{0, 1, \ldots, n\}$ and $i \in \{-1, 0, 1, \ldots, n \bmod k\}$), which are initially all set to -1, terminating with the maximum number of A winning districts in a districting of the interval $[0, j]$ in which there are exactly i long districts if such a districting exists and $i \geq 0$.

Whenever $W_i(j) \geq 0$ we define $p_i(j)$ as the starting point of the last district of one of the districtings corresponding to $W_i(j)$.

The key observation is that from an A optimal districting of an interval $[a, b]$ with a last district $[c, b]$ we get an A optimal districting for the subinterval $[a, c]$ by simply omitting last district $[c, b]$ from the districting. Consequently, $W_i(j)$ can be calculated from $W_{i-1}(j - l)$ and $W_i(j - s)$, thus the following recursion hold:

$$\begin{aligned} W_0(0) &= 0, \\ W_0(s) &= w([0, s]), \end{aligned}$$

while for $(i, j) \neq (0, 0)$ and $(i, j) \neq (0, s)$ we have $[W_i(j), p_i(j)] =$

$$\begin{cases} [W_{i-1}(j - l) + w([j - l, j]),\ j - l] & \text{if } W_{i-1}(j - l) > W_i(j - s), \\ [W_i(j - s) + w([j - s, j]),\ j - s] & \text{if } W_{i-1}(j - l) < W_i(j - s), \\ [W_i(j - s) + w([j - s, j]),\ j - s] & \text{if } W_{i-1}(j - l) = W_i(j - s) \geq 0 \text{ and} \\ & \quad w([j - s, j]) = 1, \\ [W_{i-1}(j - l) + w([j - l, j]),\ j - l] & \text{if } W_{i-1}(j - l) = W_i(j - s) \geq 0 \text{ and} \\ & \quad w([j - s, j]) = 0, \\ [-1,\ -1] & \text{if } W_{i-1}(j - l) = W_i(j - s) = -1, \end{cases}$$

where $s < j \leq n$ and $0 \leq i \leq n \bmod k$.

The values of w for short and long districts can be evaluated in linear time, while the calculation of the values $W_i(j)$ is within $\mathcal{O}(n^2)$ time complexity. Since k districts are required, the maximum number of districts party A can win is given by $W_{n \bmod k}(n)$. The values $p_i(j)$ can be used for reconstructing an optimal solution in linear time.

3.3 A Practical Approach

Since many NP-complete problems can be solved for real-life situations, we would like to point out in this section why it is difficult to find an optimal partisan districting even if only a modest number of districts have to be formed.

A real-life knapsack problem can be solved in many cases, and the number of items together with the magnitude of their values describes the complexity of the problem well. Whereas the number of districts or the number of electoral wards for districting problems can be deceptive because, while the number of districts to be drawn is relatively small, the number of possible districts is already extremely large, as we will point out in the following paragraphs.

For instance, let us consider the Hungarian Electoral System in which since 2011, Budapest has to be subdivided into 18 electoral districts from a total of 1472 wards, each serving 600-1500 voters. Thus, an average district consists of approximately 82 wards. For simplicity, we model the election map by a 2-dimensional square grid, where every cell represents a ward with a given party preference A or B. Obviously, the real-life structure is even more complex because the distribution of party A and B voters differs ward by ward, and there are further restrictions on the set of admissible districts. In this model, two cells are connected if they share a common edge, so this defines a 4-neighborhood relation on the set of cells.

Even in this simplified structure, there is no known formula for the number of

possible figures. It means, we do not know how many districts can be formed out of a given number of connected cells, so-called polyominoes. If even orientation matters, they are called fixed polyominoes. It is known that the number of polyominoes grows exponentially. Jensen [34] enumerated fixed n-cell polyominoes up to $n = 56$, which resulted in 6.9×10^{31} polyominoes for the last case, which equals the number of different shapes that can be formed out of 56 connected squares. This result shows that it is unfeasible to examine all possible cases, even for 82 wards on a Budapest scale problem. Therefore, in contrast to the knapsack problem, the number of districts to be formed in case of a districting problem underestimates the magnitude of the latter problem. Obviously, considering possible district shapes is just the first step in arriving to a districting.

It is worth noting that the dynamic programming technique applied successfully for one-dimensional districting problems in Section 3.2.1, cannot be employed in exactly the same way for the two-dimensional problems specified above since, while for the one-dimensional setting, it was possible to evaluate any important subdistricting problem by simply omitting one small or one large district, from the explanations above it follows for the two-dimensional setting that the number of possible subdistrictings will be simply too large, i.e., non-constant in the number of voters, to obtain a computationally feasible algorithm.

Another starting point to obtain a heuristic for gerrymandering, i.e., an algorithm which is not optimal but quick, would be the pack and crack principle. In a similar framework, Puppe and Tasnádi [56] showed that not every crack procedure reaches the optimal solution if geographical constraints are present. If the connectivity of the cells is not required, the problem can be easily solved by a simple crack algorithm, which leads to the optimal solution in this special case. The aim of the crack strategy for the beneficiary party is to win the query district with just the least margin, thus

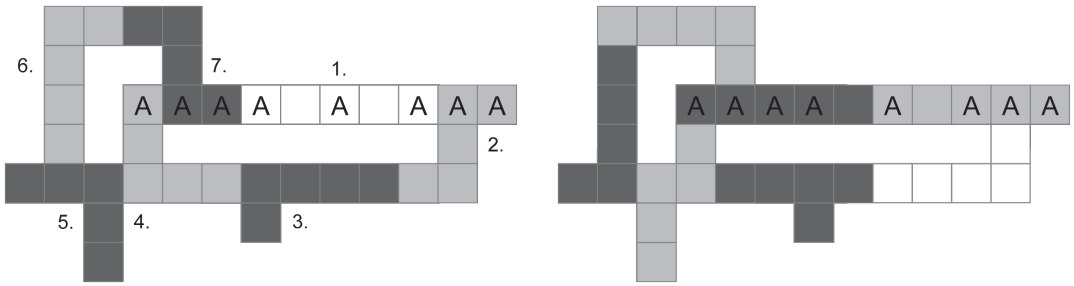

(a) Employing the crack principle. **(b)** Party A optimal districting.

Figure 3.2: Example of pack and crack principle. Source: Author.

weakening the opponent party. In fact, according to this greedy algorithm for a given district size, one has to pick just one more cell for party A than for party B if the district size is odd. Unfortunately, if we require districts to be connected, it is far from obvious how this greedy approach arrives to a feasible map tiling.

Regardless, Figure 3.2a and Figure 3.2b, contain the same gird-like geography with holes, e.g., lakes, show that employing the crack principle in favor of party A does not result in a party A optimal districting. In the unlabeled squares, we have party B voters. In particular, it can be verified that the geography depicted in Figure 3.2a and Figure 3.2b admits just these two feasible districtings from which the crack principle chooses the districting of Figure 3.2a,[5] while the party A optimal districting is shown in Figure 3.2b. Figure 3.2a and Figure 3.2b improve on the respective example in Puppe and Tasnádi [56] by pointing out that any implementation of the crack principle results for some problems in a non-partisan optimal districting.

We still might hope that by a clever combination of packing and cracking, we could obtain a party A optimal districting. The pack and crack principle requires that we draw districts sequentially in a way that the number of wasted votes by party A is decreasing, where in case of a cracked district the number of wasted votes by

[5]The numbers close to the districts indicate a possible ordering in which the districts can be chosen based on the crack principle.

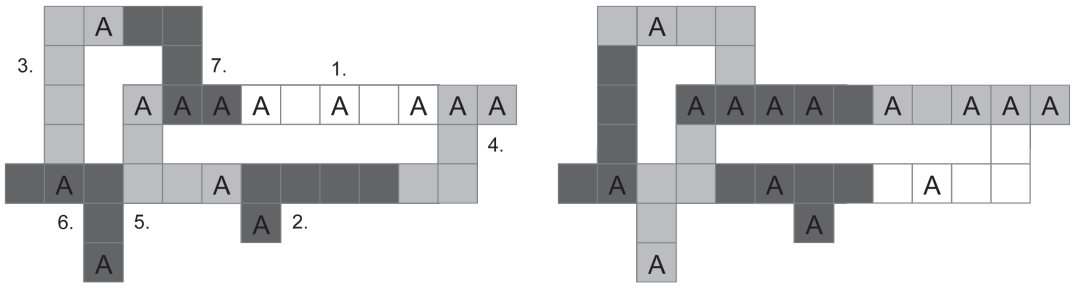

(a) Employing the pack and crack principle. **(b)** Party A optimal districting.

Figure 3.3: Another example of pack and crack principle. Source: Author.

party A equals the number of party A voters not needed for winning the respective cracked district, while in case of a packed district the number of wasted votes by party A equals the number of party A voters in the respective packed district. However, Figure 3.3a and Figure 3.3b show that the pack and crack principle does not always result in a party A optimal districting since the geography in Figure 3.3a and Figure 3.3b admits just two districtings, the pack and crack principle results in the districting depicted in Figure 3.3a, and Figure 3.3b contains the party A optimal districting.

3.4 Concluding Remarks

In this chapter, we showed that optimal partisan districting and majority securing districting in the plane with geographical constraints are NP-complete problems. To obtain a heuristic algorithm, the original problem might be simplified in some way. We provided a polynomial time algorithm for determining an optimal partisan districting for the one-dimensional version of the problem. However, to develop a procedure for finding an optimal partisan districting in general is beyond the scope of this study. We also examined a practical approach using polyominoes to give possible explanations for why finding an optimal partisan districting for real-life problems cannot be guaranteed.

Chapter 4

Measuring the Circularity of Congressional Districts

In this chapter, we continue to examine districting from a practical perspective with the help of image processing techniques. Shape analysis has special importance in the detection of gerrymandering, the manipulated redistricting. In most states of the USA, redistricting is made by non-independent actors and often causes debates about partisan manipulation. The somewhat ambiguous concept of compactness is a standard criterion for legislative districts. In the literature, circularity is widely used as a measure of compactness, since it is a natural requirement for a district to be as circular as possible. We propose a novel circularity measure based on Hu moment invariants. This parameter-free circularity measure provides a powerful tool to detect districts with abnormal shapes. We also analyze the districts of Arkansas, Iowa, Kansas, and Utah over several consecutive periods and redistricting plans, and also compared the results with some classical circularity indexes. Our findings show that the fall of the average circularity value of the new measure indicates potential gerrymandering.

Traditionally, redistricting is always contentious in the United States because it

may favor a political party. As we already mentioned in Chapter 3, redistricting has to be carried out to resolve geographical malapportionment caused by demographic changes such as migration. Gerrymandering is among the most commonly discussed practices of political manipulation. This process aims to establish a political advantage for a particular group by partially shaping district boundaries. The effort to create as compact districts as possible is a standard criterion, see, e.g., Webster[73], Polsby and Popper [54]. Hence, measuring the circularity of districts can be a suitable tool to help detect gerrymandering. This study focuses on the quantification of shape circularity. We propose a novel circularity measure based on Hu moment invariants that can be considered as a further development of the concept introduced by Nagy and Szakál [10]. We also test the new measure on various US congressional districts in different periods.

The process of redistricting is usually the following. After we determined the number of citizens belonging to one district, the boundaries have to be drawn, which is critical from the perspective of proportional representation of the voters. More details on apportionment methods can be found in Kóczy et al. [37] and [38]. Districting problems were examined by, for instance, Ricca et al. [59], Kalcsics [35], Chambers [16], Oehrlein and Haunert [52], Tasnádi [69], and Puppe and Tasnádi [55].

Several methods have been developed to measure the shape of a district, e.g., Chambers [17], Chambers and Miller [18], Young [75], Maceachren [45], and Dusek [21]. It is difficult to characterize a district with a single number because there are several correlative properties regarding the form of a planar object, e.g., circularity [1], elongation, convexity, connectivity, or the jaggedness of the boundary. These terms have different meanings in different fields of science, so there is not a common terminology for describing shapes. The standard meaning of circularity is the degree to

[1] In the literature, the terms circularity and compactness are often used interchangeably.

which a shape differs from a circle, and it is the most important index from a practical point of view. A desirable shape circularity measure should satisfy the following criteria:

- it is applicable on every planar shape,
- it ranges from 0 to 1,
- it is invariant with respect to translations, rotations, and scaling.

In the literature, measuring circularity is an accepted approach to cope with the compactness criterion that aims to limit gerrymandering. The classical circularity measures use the perimeter, the area, and various length measures of shape, but a measure that is perfect in every respect does not exist. The most widespread indexes are, e.g., the Reock Test (RT) [58], the Polsby-Popper Test (PPT) [54], and the Lee-Sallee Index (LSI) [39].

Image moments are used in image processing to characterize shapes. These moments are invariant to similarity transformations and can be calculated effectively. Initially, moment-based circularity measure was introduced by Žunić [77], Žunić et al. [78], and Nayak and Stojmenovic [50]. Many attempts have been made in order to detect gerrymandering, e.g., Ansolabehere and Palmer [4]. A method for evaluating the shape of political districts based on geometric characteristics and comparison with ranking established by human judgment can be found in Lunday [43]. In Fan et al. [22], the authors analyzed the compactness of redistricting plans in California and North Carolina by calculating four compactness measures, including some classical indexes.

In Nagy and Szakál [10], we studied the shape of the congressional districts by a measure C_β that depended on a parameter β. This index is invariant under similarity transformations, and its sensitivity to lacerated boundaries is adjustable by β. The

measure was evaluated for several parameters and they were compared with the LSI, the PPT, RT on actual US congressional districts. We reached the conclusion that $\beta = 2$ is an appropriate parameter on the sample set. Thanks to the Hu moment invariants, the evaluation of this measure was efficient to set against other indexes.

Sziklai and Héberger [68] compared our measure with the three classical circularity measures (RT, LSI , PPT) by the so-called Sum of Ranking Differences method. This novel statistical approach ranks competing solutions based on a reference point. It is rapidly gaining popularity in various fields of science, from analytical chemistry to finance. Their analysis concluded that LSI and our measure with the suitable parameters performed the best.

However, as it has been revealed in Nagy and Szakál [9], when we compared the circularity of two districts with different β parameters, the circularity order changed in certain cases, which is an undesirable feature of the index. Thus, we aimed to develop the C_β measure and introduce a more robust index M that does not need any parameters. We found that this new measure provides a powerful method to detect districts with abnormal shapes. Examining several consecutive periods show that the fall of average circularity can indicate gerrymandering.

This chapter is organized as follows. In Section 4.1, the outline of moment invariants can be found. Section 4.2 gives a brief overview of circularity measures. Section 4.3 reveals an unpleasant feature of C_β and demonstrates the application of the new circularity measure M on congressional districts of Arkansas, Iowa, Kansas, and Utah. Finally, our conclusions are drawn in Section 4.4.

4.1 Moment Invariants

Moment invariants are widely used in pattern recognition and have been studied in the literature, for instance, Csetverikov [20], Hu [32], Žunić et al. [78], and Nayak

and Stojmenovic [50]. Our proposed circularity measure uses moment invariants for shape analysis. The most important notions will be reviewed below.

Definition 4.1.1. *Let $gm_{p,q}(D)$ be the geometric moment of order (p+q) of a planar shape D*

$$gm_{p,q}(D) = \int\int_D x^p y^q dxdy,$$

where $(p, q = 0, 1, 2, ...)$.

The examined objects consist of pixels, so typically, the discrete version of Definition 4.1.1 is applied.

Definition 4.1.2. *Let $GM_{p,q}(D)$ be the (discrete) geometric moment of order (p+q) of a planar shape D*

$$GM_{p,q}(D) = \sum_{(i,j)\in D\cap\mathbb{Z}^2} i^p j^q,$$

where $(p, q = 0, 1, 2, ...)$ and $\mathbb{Z}$ is the set of integers.

Definition 4.1.3. *Let $im_{p,q}(D)$ be the image moment of order (p+q) of a planar shape D*

$$im_{p,q}(D) = \int\int_D x^p y^q f(x, y)\, dxdy,$$

where $f(x, y)$ is the brightness function of the image and $(p, q = 0, 1, 2, ...)$.

The discrete version of Definition 4.1.3 can be defined as follows.

Definition 4.1.4. *Let $IM_{p,q}(D)$ be the (discrete) image moment of order (p+q) of a planar shape D*

$$IM_{p,q}(D) = \sum_{(i,j)\in D\cap\mathbb{Z}^2} i^p j^q f(i, j),$$

where $f(x, y)$ is the brightness function of the image, $(p, q = 0, 1, 2, ...)$ and $\mathbb{Z}$ is the set of integers.

The brightness function is usually normalized into 0 to 1, and can be interpreted as a probability density function of a 2D random variable. The brightness of a grayscale image can be characterized by image moments, so we use them to describe the shape of congressional districts. In future research, the brightness function could be applied for representing the population density over an area.

Let $(\overline{x}, \overline{y})$ be the centroid of the image that can be obtained by normalization of the first order moments:

$$\overline{x} = \frac{IM_{1,0}(D)}{IM_{0,0}(D)}, \quad \overline{y} = \frac{IM_{0,1}(D)}{IM_{0,0}(D)}.$$

By shifting the centroid to the origin, a moment that is invariant with respect to the location of the shape can be constructed. Thus, the central image moments can be defined as follows.

Definition 4.1.5. *Let $\mu_{p,q}(D)$ be the central image moment of order (p+q) of a planar shape D*

$$\mu_{p,q}(D) = \int \int_D (x - \overline{x})^p (y - \overline{y})^q f(x, y) \, dxdy,$$

where $f(x, y)$ is the brightness function of the image and $(p, q = 0, 1, 2, ...)$.

We also define the discrete version of Definition 4.1.5.

Definition 4.1.6.

$$\mu_{p,q}(D) = \sum_{(i,j) \in D \cap \mathbb{Z}^2} (i - \overline{x})^p (j - \overline{y})^q f(i, j),$$

where $f(x, y)$ is the brightness function of the image, $(p, q = 0, 1, 2, ...)$ and $\mathbb{Z}$ is the set of integers.

Moments also have physical meaning. For instance, it is easy to see that $IM_{0,0}(D)$ represents the entire intensity of the image, while $\mu_{2,0}(D)$ and $\mu_{0,2}(D)$ are the variance of the brightness function. These quantities will play an essential role in the future.

Definition 4.1.7. *Let $\eta_{p,q}(D)$ be the normalized central image moment of order (p+q) of a planar shape D*

$$\eta_{p,q}(D) = \frac{\mu_{p,q}(D)}{\mu_{0,0}(D)^{\gamma}},$$

where

$$\gamma = 1 + \frac{p+q}{2}.$$

With the help of the normalized central moments, Hu ([32]) introduced seven moments that are invariant under translations, rotations and scaling. In our study we are focusing on the first Hu moment invariant:

Definition 4.1.8. *Let $\phi_1(D)$ be the first Hu moment invariant of a planar shape D*

$$\phi_1(D) = \eta_{2,0}(D) + \eta_{0,2}(D).$$

4.2 Circularity Measures

Measuring the compactness of congressional districts can be a powerful tool in gerrymandering detection. Unsurprisingly, the definition of many shape descriptors is based on the degree to which a shape differs from a circle.

The following requirements hold for a circularity measure C:

1. $C(D) \in (0, 1]$ for any planar shape D;
2. $C(D) = 1$ if and only if D is a circle;
3. $C(D)$ is invariant with respect to similarity transformations (translations, rotations and scaling);
4. For each $\delta > 0$ there is a shape D such that $0 < C(D) < \delta$, i.e., there are shapes whose measured circularity are arbitrarily close to 0.

There are a large number of shape descriptors in the literature that can be applied as a circularity measure for a region, and there are several attempts to classify them into different categories, see Maceachren [45] and Niemi et al. [51].

In this section, we will briefly introduce the most commonly used shape descriptors. In Definition 4.2.6, we introduce a new circularity measure based on the concept that is defined in Definition 4.2.5.

4.2.1 Classical Circularity Indexes

One of the most popular contour-based indexes is the PPT. It compares the area of the shape D to the area of a circle that has the same perimeter as the shape.

Definition 4.2.1. *Let the measure $C_{PP}(D)$ be the Polsby-Popper Test for a planar shape D*

$$C_{PP}(D) = \frac{4\pi \cdot area(D)}{perimeter(D)^2}.$$

It can be easily checked that this definition satisfies the above-mentioned properties.

The next one is a famous area-based measure, the RT, which finds the smallest circle O containing the district D and takes the ratio of its area to that of the circle.

Definition 4.2.2. *Let the measure $C_R(D)$ be the Reock Test for a planar shape D*

$$C_R(D) = \frac{area(D)}{area(O)}.$$

Another possible way to quantify the circularity of a shape is to place a reference shape R on the examined shape D making sure that the overlapping area is maximal. According to the practice, we arrange the two shapes that their centroids coincide, and we use a circle O as a reference shape. Thus we get the following circularity measure.

Definition 4.2.3. *Let the measure $C_{LS}(D)$ be the Lee-Sallee Index for a planar shape D*

$$C_{LS}(D) = 1 - \frac{area(D \bigtriangleup O)}{area(D \cup O)} = \frac{area(D \cap O)}{area(D \cup O)},$$

where circle O is a reference shape that has an equal area to D and $\bigtriangleup$ is the symmetric difference.

4.2.2 Moment Invariants as Circularity Measures

Let us assume that all the examined shapes are compact in the topological sense, which does not restrict our image processing task. Besides, we analyze the shape of a congressional district and do not take the population into account. The brightness function can be considered as the indicator function. Before we introduce our novel circularity measure, two definitions shall be recalled here. Proposition 4.2.1 and Definition 4.2.4 are from Žunić et al. [78].

Proposition 4.2.1. *Let D be a compact planar shape. Then*

$$\phi_1(D) = \eta_{2,0}(D) + \eta_{0,2}(D) = \frac{\mu_{2,0}(D) + \mu_{0,2}(D)}{\mu_{0,0}(D)^2} \geq \frac{1}{2\pi}$$

$$\phi_1(D) = \eta_{2,0}(D) + \eta_{0,2}(D) = \frac{\mu_{2,0}(D) + \mu_{0,2}(D)}{\mu_{0,0}(D)^2} = \frac{1}{2\pi} \iff \textit{if } D \textit{ is a circle.}$$

Based on Proposition 4.2.1 a circularity measure C_1 can be constructed as follows.

Definition 4.2.4. *Let D be a compact planar shape and the area of circle O equals to the area of D. Then $C_1(D)$ is a circularity measure*

$$C_1(D) = \frac{\phi_1(O)}{\phi_1(D)} = \frac{1}{2\pi} \cdot \frac{\mu_{0,0}(D)^2}{\mu_{2,0}(D) + \mu_{0,2}(D)}.$$

It is easy to see that this circularity measure satisfies the required properties. Using normalized central moments, we get moments invariant with respect to scaling. If the scale factor is λ, then the new central moments are:

$$\mu'_{p,q} = \lambda^{p+q+2} \cdot \mu_{p,q}.$$

Specially,

$$\mu'_{0,0} = \lambda^2 \cdot \mu_{0,0}.$$

Hence it follows that,

$$\eta'_{2,0} = \frac{\mu'_{2,0}}{\left[\mu'_{0,0}\right]^2} = \frac{\lambda^4 \cdot \mu_{2,0}}{\left[\lambda^2 \cdot \mu_{0,0}\right]^2} = \eta_{2,0}\,,$$
$$\eta'_{0,2} = \frac{\mu'_{0,2}}{\left[\mu'_{0,0}\right]^2} = \frac{\lambda^4 \cdot \mu_{0,2}}{\left[\lambda^2 \cdot \mu_{0,0}\right]^2} = \eta_{0,2},$$

which verifies the scale invariance of the central moments.

After rotating the shape by an angle of α, the second order moment can be expressed in the following way:

$$\mu'_{2,0} = \cos^2\alpha \cdot \mu_{2,0} + \sin^2\alpha \cdot \mu_{0,2} - \sin 2\alpha \cdot \mu_{1,1},$$
$$\mu'_{0,2} = \sin^2\alpha \cdot \mu_{2,0} + \cos^2\alpha \cdot \mu_{0,2} + \cos 2\alpha \cdot \mu_{1,1}.$$

Thus

$$\mu'_{2,0} + \mu'_{0,2} = \left(\sin^2\alpha + \cos^2\alpha\right)\left(\mu_{2,0} + \mu_{0,2}\right) = \mu_{2,0} + \mu_{0,2},$$

that is

$$\phi'_1 = \phi_1.$$

In Hu [32], the proof of translation and rotation invariance can also be found.

The following circularity measure C_β from Žunić et al. [78] is a generalization of C_1, and it is applicable in special cases when we want to set the sensitivity manually for

a specific purpose. We applied this circularity measure for measuring the circularity of congressional districts for the first time in Nagy and Szakál [10].

Definition 4.2.5. *Let D be a planar shape whose centroid coincides with the origin and let β be a real number greater than -1 and $\beta \neq 0$. Then $C_\beta(D)$ is the generalized moment-based circularity measure*

$$C_\beta(D) = \begin{cases} \dfrac{\mu_{0,0}(D)^{\beta+1}}{\pi^\beta(\beta+1)\displaystyle\int\int_D \left(x^2+y^2\right)^\beta dxdy} & \text{if } \beta > 0 \\ \dfrac{\pi^\beta(\beta+1)\displaystyle\int\int_D \left(x^2+y^2\right)^\beta dxdy}{\mu_{0,0}(D)^{\beta+1}} & \text{if } \beta \in (-1,0). \end{cases}$$

Nevertheless, we revealed an undesired feature of this measure, which emerged from the examined data. The circularity order can change when we apply different β parameters to dissimilar shapes, as it is highlighted in Figure 4.4 and Figure 4.5. That is the main reason why we should take multiple β parameters into account at the same time. Besides, our goal is to describe district circularity by a single value and make a comparison with other districts or with other periods. Therefore, in the next definition, we propose the normalized measure of the area under the curve of C_β for $\beta \in (-1,0) \cup (0,\infty)$ as a novel circularity measure and denote it by M.

Definition 4.2.6. *Let $C_\beta(D)$ be the generalized moment-based circularity measure. Then M is a circularity measure*

$$M(D) = \lim_{b\to\infty} \frac{1}{b+1} \int_{-1}^{b} C_\beta(D)\, d\beta.$$

In fact, M equals the average of C_β for β. Furthermore, it also keeps the beneficial properties of C_β, and it is more robust in some cases. Figure 4.1 illustrates the different characteristics of C_β on two dissimilar shapes, and it also shows the circularity values of the classical indexes and the new measure M. More details on the application of the new measure will be given in the following section.

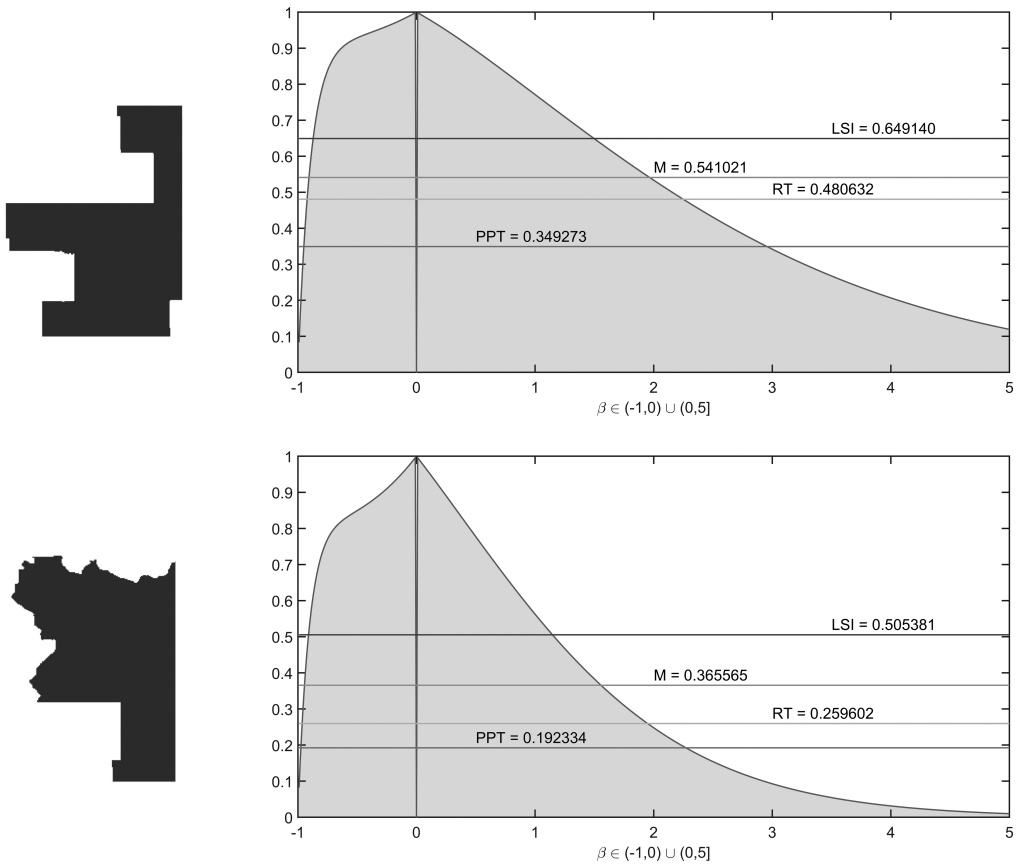

Figure 4.1: The C_β curve and the comparison of M with the classical circularity indexes on two dissimilar shapes. Source: Author.

4.3 Application of the New Circularity Measure

The United States Congress consists of two chambers, the Senate and the House of Representatives. The 50 states have been divided into a total of 435 congressional districts in the House of Representatives, with each one representing approximately 711 thousand citizens. The US Congress has 535 voting members, 435 Representatives, and 100 Senators. The members of the House of Representatives serve two-year terms representing the people of a congressional district. The Census Bureau within the United States Department of Commerce conducts a decennial census, and the results of it are used to determine the boundaries of the districts. The boundaries can

be redrawn, e.g., two districts can be merged into one, see Iowa from 113^{th} Congress, or a district can be separated into two districts, see Utah from 113^{th} Congress. Surprisingly, in most states, this process is made by non-independent actors and often causes debates about partisan manipulation. According to Levitt [40], only a few states have an independent commission that draws the district lines because state legislatures usually have primary control over the congressional lines in their state.

Unfortunately, the definition of compactness is not clear-cut, see Chambers and Miller [17]. However, the measure of how far the points of the district is from the center, determined by classical circularity indexes is essential in redistricting. [2] In some cases, there is a *prima facie* evidence that a district is manipulated, see the famous example of Illinois 4/107 in Figure 4.6. On the other hand, it is hard to determine the ideal shape for a congressional district. Moreover, as we discussed in Chapter 3, the optimal partisan redistricting is also difficult.

4.3.1 The Computation of the Measures

In order to determine the circularity measures, some image processing tasks should be carried out on the cartographic shapefiles that were retrieved from US Census Bureau [71]. We rendered the vector maps of the selected states to grayscale bitmap images by QGIS. Thus, the different areas could be separated by the pixel intensity values by MATLAB. A simple example for the operation of the algorithm can be seen in Figure 4.2a, the white area is the examined district, black is the rest of the state, and gray is an ignorable region, e.g., sea or a neighboring state. Then we calculate the centroid of the district with the help of the central moments. This allows us to determine the reference circle, as Figure 4.2b shows. The area of the reference circle

[2] Interestingly, Arkansas does not require congressional or legislative districting plans to be compact.

equals to the area of the district being investigated. Finally, we need the Hu moment invariants to determine the new circularity measure. The classical circularity indexes that we use for comparison only require the area and perimeter of the shape.

(a) Input of the algorithm. **(b)** The corresponding reference circle.

Figure 4.2: The computation of the new measure M. Source: Author.

4.3.2 An Undesired Feature of the Moment-based Circularity Measure

The moment-based circularity measure C_β was first applied for analyzing the shape of congressional districts in Nagy and Szakál [10], where we examined the measure as a function of β, Figure 4.3 shows an example for $\beta = -0.5, 1, 2, 8$. We also compared the values of C_β with the PPT, RT, and LSI on various congressional districts. We will also use these indexes as benchmarks when we try to detect gerrymandering.

However, our research revealed in certain cases, when we compare the circularity of two districts with different β parameters, the order changed, which is an undesired feature of the circularity index. Figure 4.4 presents the case of $\beta = -0.5$ for two districts where $AR03/107$ is more circular than $AR01/113$, while for $\beta = 1$ it is just the opposite. This phenomenon appears in a more relevant part of the domain, between 1 and 2, as it can be seen in Figure 4.5. That was one of the reasons why we introduced the new index M defined in Definition 4.2.6. The other beneficial property of M that it does not require any parameters.

β	$C_\beta(AR02/107)$	$C_\beta(KS04/107)$
-0.5	0.9235	0.9226
1	0.6401	0.6550
2	0.3013	0.3321
8	0.0008	0.0014

(a) AR02/107. **(b)** KS04/107.

Figure 4.3: Comparison the circularity of two districts by C_β. Source: Author.

β	$C_\beta(AR03/107)$	$C_\beta(AR01/113)$
-0.5	0.9404	0.9059
1	0.6977	0.7159

(a) AR03/107. **(b)** AR01/113.

Figure 4.4: Arkansas's 3^{rd} district in the 107^{th} and 1^{st} district in the 113^{th} Congress. Source: Author.

Finally, an illustration that shows the nature of the examined circularity measures, in a nutshell, can be found in Figure 4.6. In this example, we can see the circularity evaluation of two diversiform districts. The fourth district of Illinois in the 107^{th} Congress is a famous example of gerrymandering, with its tangled boundaries and

small area compared to its perimeter, has much lower circularity than Arkansas second district from the 113^{th} Congress. The different characteristic of the two curves is distinctly visible as β changes. In the upper instance, $C_\beta(D)$ curve decreases much slower compared to the lower case. Furthermore, the more irregular the shape is, the faster the value converges to 0, for details see Žunić et al. [78]. This example also shows that determining an appropriate β for C_β is not straightforward. PPT, RT, and LSI all fall into the interval of $\beta \in [1, 3]$. Therefore, we applied $\beta = 2$ in Nagy and Szakál [10]. However, Definition 4.2.6 proposes a more robust solution, instead of choosing a specify β, we take the area under the curve C_β and yield the new circularity measure M.

$\boldsymbol{\beta}$	$\boldsymbol{C_\beta(AO01/107)}$	$\boldsymbol{C_\beta(IO02/108)}$
1	0.7900	0.7712
2	0.5271	0.5335

(a) IO01/107. **(b)** IO02/108.

Figure 4.5: Iowa's 1^{st} district in the 107^{th} and 2^{nd} district in the 108^{th} Congress. Source: Author.

4.3.3 Detection of Gerrymandering

When we try to detect gerrymandering, we should consider the average circularity of a state through successive Congresses and seek significant anomalies. Thus, we can

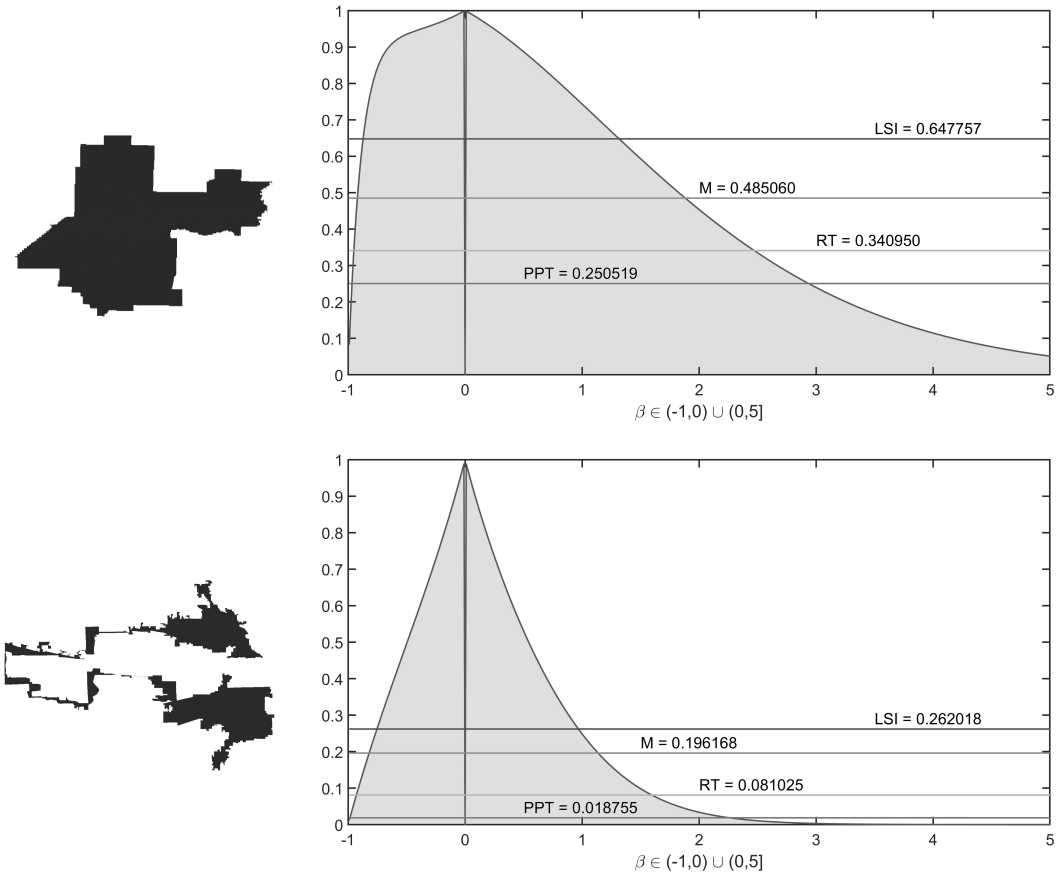

Figure 4.6: The C_β curve and the comparison of M with the classical circularity indexes on Arkansas's 2^{nd} district in the 113^{th} and Illinois's 4^{th} district in the 107^{th} Congress.

track the changes and reduce the impact of external conditions, e.g., geographical constraints. We have analyzed four states in the period of the 107^{th} (from January 3, 2001, to January 3, 2003), 108^{th} (from January 3, 2003, to January 3, 2005) and 113^{th} (from January 3, 2013, to January 3, 2015) US Congress. The populations of these states are similar, around 3 million, and they all have 3 to 5 districts. See Figure 4.7 for the overview map of Arkansas, Iowa, Kansas and Utah in the 113^{th} Congress. The summary of the experimental results can be found in Figure 4.8, Figure 4.9 [3], Figure

[3]Since 2013, there are only 4 districts in this state.

4.10, and Figure 4.11 [4]. More details on this will be given in Appendix B, and they can be also seen on an interactive map, see Nagy and Szakál [8].

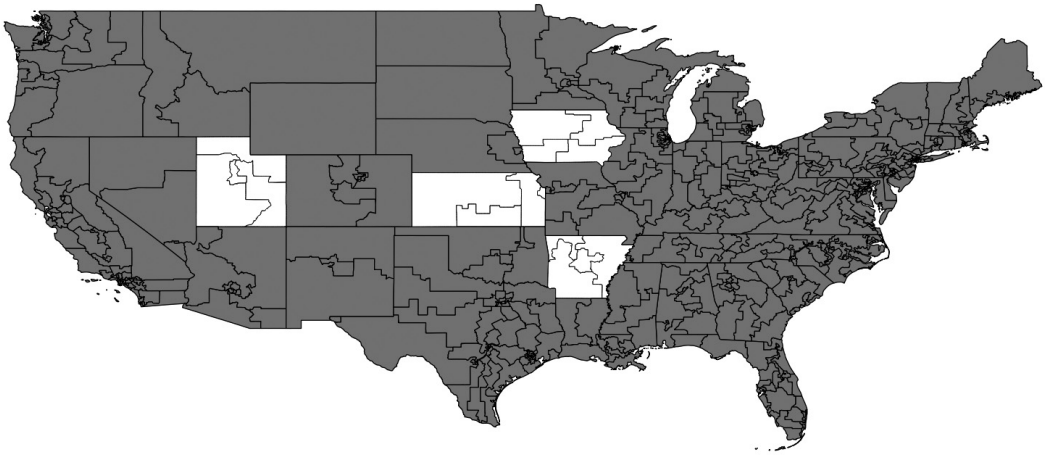

Figure 4.7: The boundaries of the 113^{th} Congress. Arkansas, Iowa, Kansas and Utah are highlighted. Source: Author.

All circularity indexes of Utah decreased in stages from the 107^{th} to the 113^{th} Congress. In Iowa, the examined indexes behaved similarly in these periods, the 107^{th} showed the best, while 108^{th} worst results. In Arkansas, LSI and PPT decreased monotonically while RT and M had a peak at 108^{th}. Remarkably, M was more sensitive to the change than RT. The most interesting state was Kansas, where the indexes gave completely different orders, and M was the only one with a falling trend.

An example of presumable gerrymandering is given below. Figure 4.12 shows the third district of Arkansas alone through the 107^{th}, 108^{th} and the 113^{th} Congress. In the table, we can see an almost unambiguous improvement in the circularity values from the 107^{th} to the 108^{th} period, then a major fall from the 108^{th} to the 113^{th} Congress, which gives rise to suspicion of gerrymandering. The strange shape of the district in the last period is also visible to the naked eye.

[4]Since 2013, there are already 4 districts in this state.

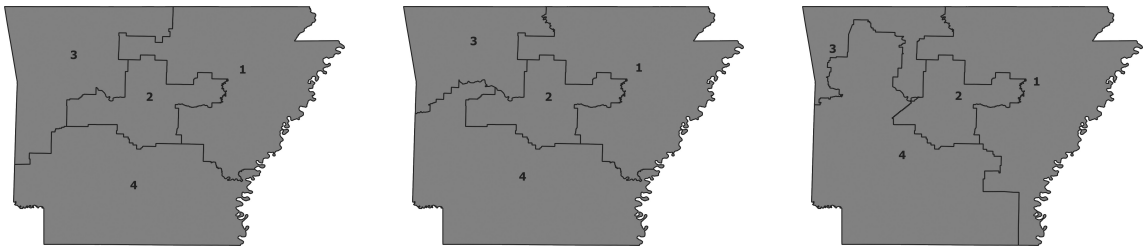

Measure	M			LSI			RT			PPT		
District \ Congress	107	108	113	107	108	113	107	108	113	107	108	113
1	0.5619	0.5678	0.4536	0.7206	0.7005	0.6316	0.3955	0.4310	0.3003	0.1436	0.1426	0.1051
2	0.4061	0.4062	0.4851	0.5816	0.5819	0.6478	0.3107	0.3106	0.3410	0.2207	0.2212	0.2505
3	0.4398	0.5391	0.2648	0.6192	0.6569	0.2745	0.3281	0.4406	0.2812	0.3266	0.3200	0.1291
4	0.5045	0.4830	0.4787	0.6165	0.5736	0.6293	0.3938	0.3918	0.3855	0.2605	0.2151	0.2685
Average	0.4781	0.4990	0.4206	0.6345	0.6282	0.5458	0.3570	0.3935	0.3270	0.2378	0.2247	0.1883

Figure 4.8: The congressional of Arkansas districts for the 107^{th}, 108^{th} and the 113^{th} US Congresses. Source: Author.

4.4 Concluding Remarks

This chapter has investigated the shape circularity of congressional districts. The circularity of a district is a fundamental requirement by citizens, and unsurprisingly, it is also included in the regulation of many states. The measure presented by Nagy and Szakál [10] performed well compared with classical circularity indexes. However, later we found several instances where the circularity order of the districts changed after different β parameters were applied. We have made some improvements to this measure and create a more robust method that does not depend on any parameters. Our experiments on US congressional districts confirmed that the new index is useful, and in many cases, it is more sensitive than the traditional circularity measures.

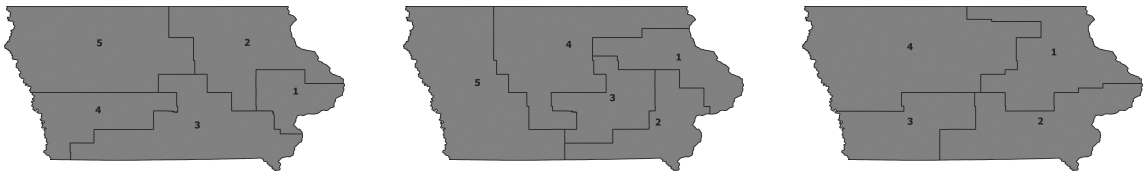

Measure	M			LSI			RT			PPT		
District \ Congress	107	108	113	107	108	113	107	108	113	107	108	113
1	0.5285	0.3395	0.3384	0.6552	0.5103	0.4616	0.3882	0.2024	0.2330	0.4032	0.2619	0.2725
2	0.3375	0.5410	0.4312	0.4834	0.6491	0.5410	0.2084	0.4806	0.3716	0.2547	0.3493	0.4024
3	0.3585	0.4477	0.4483	0.4450	0.5563	0.5797	0.2544	0.3404	0.2983	0.3023	0.3218	0.3649
4	0.5099	0.3798	0.4515	0.6095	0.5464	0.6186	0.4280	0.2179	0.3108	0.4680	0.2844	0.2379
5	0.4545	0.3268		0.6540	0.4269		0.2725	0.2378		0.3231	0.3027	
Average	0.4378	0.4070	0.4174	0.5694	0.5378	0.5502	0.3103	0.2958	0.3034	0.3503	0.3040	0.3194

Figure 4.9: The congressional districts of Iowa for the 107^{th}, 108^{th} and the 113^{th} US Congresses. Source: Author.

Measure	M			LSI			RT			PPT		
District \ Congress	107	108	113	107	108	113	107	108	113	107	108	113
1	0.4778	0.4690	0.4197	0.7902	0.7766	0.6344	0.3867	0.3321	0.3694	0.4312	0.3856	0.3987
2	0.3936	0.4216	0.4053	0.4388	0.4892	0.4819	0.3549	0.3776	0.3322	0.2300	0.2440	0.3362
3	0.4918	0.4305	0.5606	0.6119	0.6102	0.6973	0.3893	0.3330	0.4396	0.3550	0.2861	0.4440
4	0.4214	0.4071	0.3315	0.5486	0.5444	0.3774	0.3455	0.3148	0.3198	0.4673	0.4490	0.3759
Average	0.4462	0.4321	0.4293	0.5974	0.6051	0.5478	0.3691	0.3394	0.3653	0.3709	0.3412	0.3887

Figure 4.10: The congressional districts of Kansas for the 107^{th}, 108^{th} and the 113^{th} US Congresses. Source: Author.

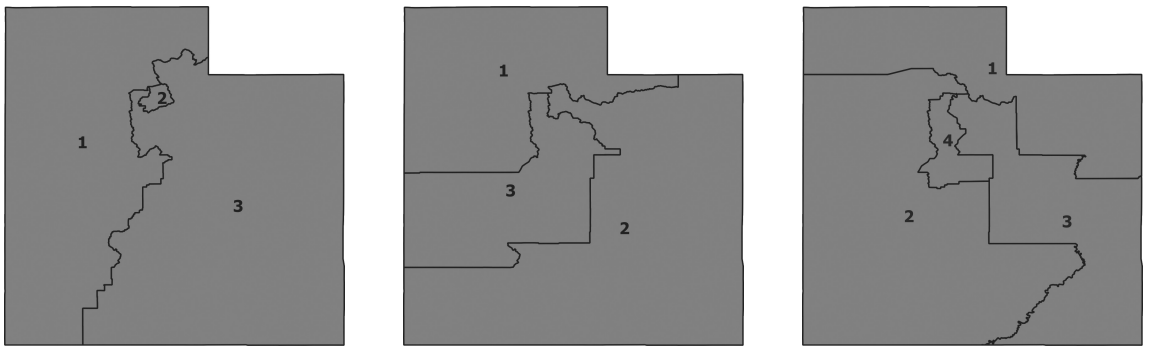

Measure	M			LSI			RT			PPT		
District \ Congress	107	108	113	107	108	113	107	108	113	107	108	113
1	0.4121	0.4993	0.2726	0.5058	0.6832	0.2909	0.3386	0.2803	0.2158	0.3196	0.3549	0.2666
2	0.6576	0.4198	0.5609	0.7474	0.5681	0.6466	0.4823	0.3108	0.4711	0.3471	0.3034	0.3364
3	0.5675	0.4607	0.3655	0.7003	0.5350	0.5054	0.5134	80.3989	0.2596	0.3334	0.3023	0.1923
4			0.3748			0.4898			0.3131			0.2200
Average	0.5457	0.4599	0.3935	0.6512	0.5954	0.4832	0.4448	0.3300	0.3149	0.3334	0.3202	0.2538

Figure 4.11: The congressional districts of Utah for the 107^{th}, 108^{th} and the 113^{th} US Congresses. Source: Author.

(a) AR03/107. **(b)** AR03/108. **(c)** AR03/113.

Index \ Congress	107^{th}	108^{th}	113^{th}
LSI	0.6192	0.6569	0.2745
RT	0.3281	0.4406	0.2812
PPT	0.3266	0.3200	0.1291
M	0.4398	0.5391	0.2648

Figure 4.12: The evaluation of Arkansas's 3^{rd} district in the 107^{th}, 108^{th} and 113^{th} US Congresses by M and the classical circularity indexes. Source: Author.

Chapter 5

Conclusion

In this thesis, we discussed problems from the fields of computer vision and congressional districting. The connection between the two seemingly distant subjects is image processing, which can be applied for both skyline extraction and circularity measurement. Computer vision determines the properties of the 3D world from images. In pattern recognition tasks, we often use image moments to summarize or describe shapes. Hu moment invariants proved to be a useful tool in analyzing the shape of political districts that plays an important role in the detection of gerrymandering.

In Part I, we started with the examination of a real-world computer vision problem, where the experimental results showed that the developed solution could be integrated into a hiking application.

In Chapter 2, we introduced an effective method for improving orientation in an AR mobile application by using a mountainous skyline. These apps have a serious problem with the accuracy of the azimuth angle provided by the digital magnetic compass sensor of the device since it is prone to interference when using it near metal objects or electric currents. With the camera and a DEM, we could determine the correct orientation angles without manual interaction. This chapter focuses on an automatic edge-based skyline extraction method that can be used for orientation in

mountainous terrain. We extracted the skyline from the image in multiple steps, and we also defined a target function to select the skyline from candidates. The proposed algorithm performed well on the sample set. Then, we carried out field tests to verify the accuracy of the method in a real-world environment. These tests showed that the azimuth angles provided by the algorithm were 1.04° on average from the ground truth azimuth. The publication related to Chapter 2 is Nagy [7].

In Part II, we turned to districting problems, and we presented a theoretical and a more empirical study. These studies address issues that have significant importance to society.

In Chapter 3, we studied the districting problem from a theoretical point of view. We showed that optimal partisan districting and majority securing districting in the plane with geographical constraints are NP-complete problems, and we provided a polynomial time algorithm for determining an optimal partisan districting for a simplified version of the problem. Besides, we gave possible explanations for why finding an optimal partisan districting for real-life problems cannot be guaranteed by a practical approach that using polyominoes. The publication related to Chapter 3 is Fleiner et al. [26].

In Chapter 4, we presented an empirical study on gerrymandering. Shape analysis has special importance in the detection of manipulated redistricting. We applied techniques widely used in computer vision, and with the help of them, we introduced a novel, parameter-free circularity measure M based on Hu moment invariants. Then, we analyzed the shape of Arkansas, Iowa, Kansas, and Utah after redistricting through multiple US Congresses, and we compared the values with some classical circularity measures. The experimental results showed that our method could indicate suspected cases of gerrymandering. The publications related to Chapter 4 are Nagy and Szakál [10] and [9].

It is worth mentioning that we also have some ongoing researches that, to a certain extent, are related to the topic of this thesis.

The first one is another application of computer vision. Traffic enforcement cameras can classify vehicles, recognize license plate numbers, detect speeding, and automatically send tickets to the offenders. Fastened seat belts can save lives and play an important role in decreasing casualties of traffic accidents. Therefore seat belt detection is an essential but quite a complex task. Due to external circumstances, the image quality is often poor, sometimes, even a human observer can hardly decide whether the seat belt is fastened or not. We propose a novel method that can support the decision of authorities by selecting drivers who do not use their seat belts. We use edge detection and Hough transformation to find parallel line segments, then we train an artificial neural network with the extracted features. Preliminary experiments show that this method could be the base of a forthcoming traffic surveillance system.

The next one is a theoretical study in which we use computer simulations in a socially relevant problem. In Nagy and Tasnádi [11], we investigate the presence of a socially concerned firm in the framework of a Bertrand-Edgeworth duopoly with capacity constraints. In particular, we determine the mixed-strategy equilibrium of this game and relate it to both the standard and the mixed versions of the Bertrand-Edgeworth game. In this model, the government tries to regulate a market by obtaining partial ownership in a firm. This type of socially concerned firm behaves as a combined profit and social surplus maximizer. In contrast to other results in the literature, we find that full privatization is the socially best outcome that is the optimal level of public ownership is equal to zero. However, the deduction of this result is complicated, thus first, we use simulations that help to find equilibria in our model.

Finally, we have an R&D project that aims to use high-resolution hand-motion

data of individuals while writing their signatures to identify them securely. We developed a novel pen-sized device that could capture the dynamic details of a signature. The pen is equipped with a 3-axial accelerometer, 3-axial gyroscope, and also a pressure sensor. The hardware has an optical-based tamper resistance method that protects from physical manipulation. We test several algorithms to match signatures. Firstly, a dynamic time warping-based approach which is a classical method in online signature verification. Secondly, a statistical method based on the distribution of the values of the prepared data. Finally, a neural network-based method where a feed-forward multi-layer perceptron was trained for each signatory for detecting fake signatures by analyzing the signals. In such a system, the False Acceptance Rate should be as low as possible, while the False Rejection Rate is just inconvenient for the user.

Appendix A

Skyline Extraction

Appendix A presents the steps of automatic skyline extraction on four challenging examples. Cragged mountain ridges or the cloudy sky could cause a problem for an algorithm. These examples demonstrate the proposed method's efficiency.

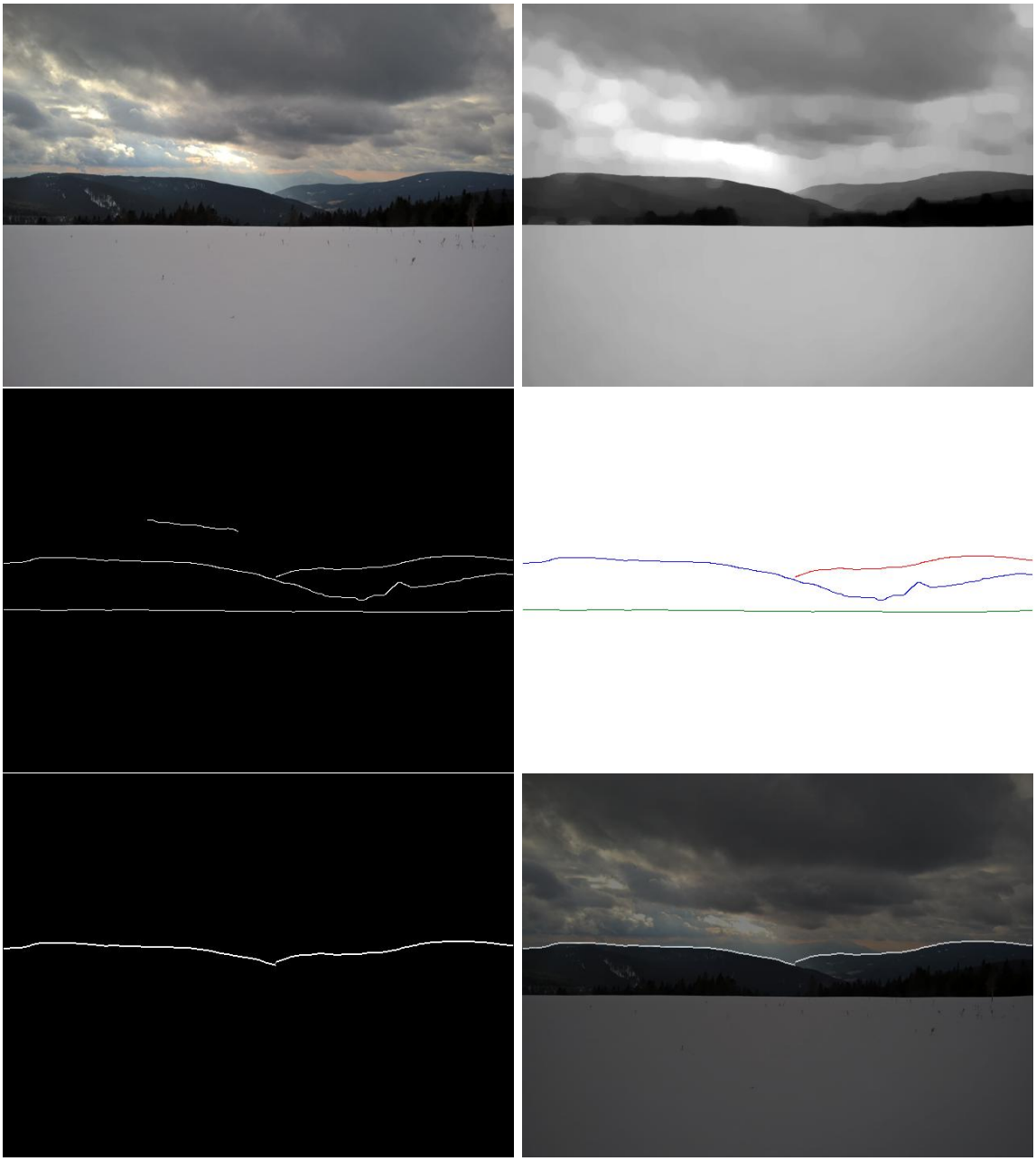

Figure A.1: Example for skyline extraction. Source: Author.

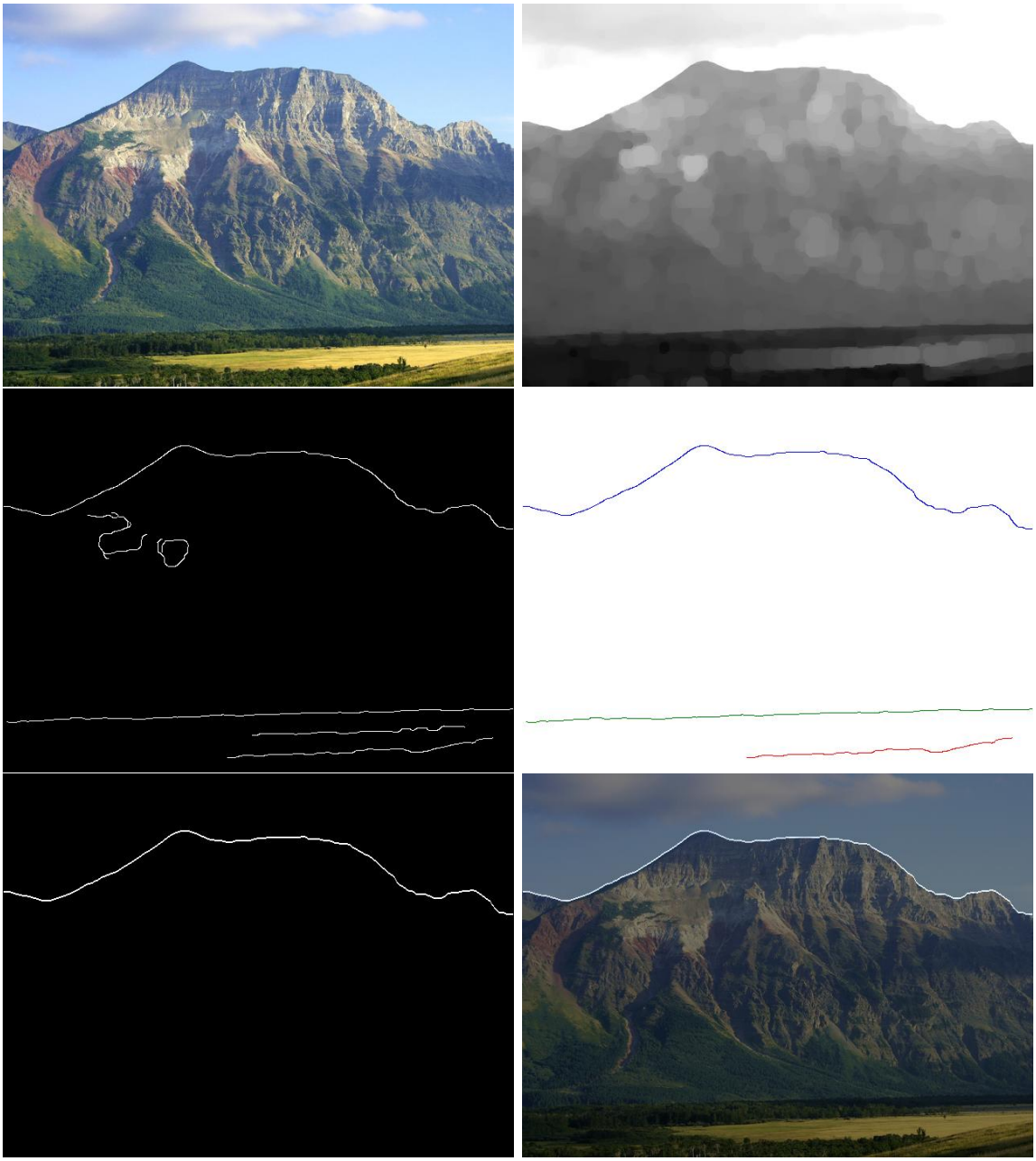

Figure A.2: Example for skyline extraction. Source: Flickr Creative Commons.

Figure A.3: Example for skyline extraction. Source: Flickr Creative Commons.

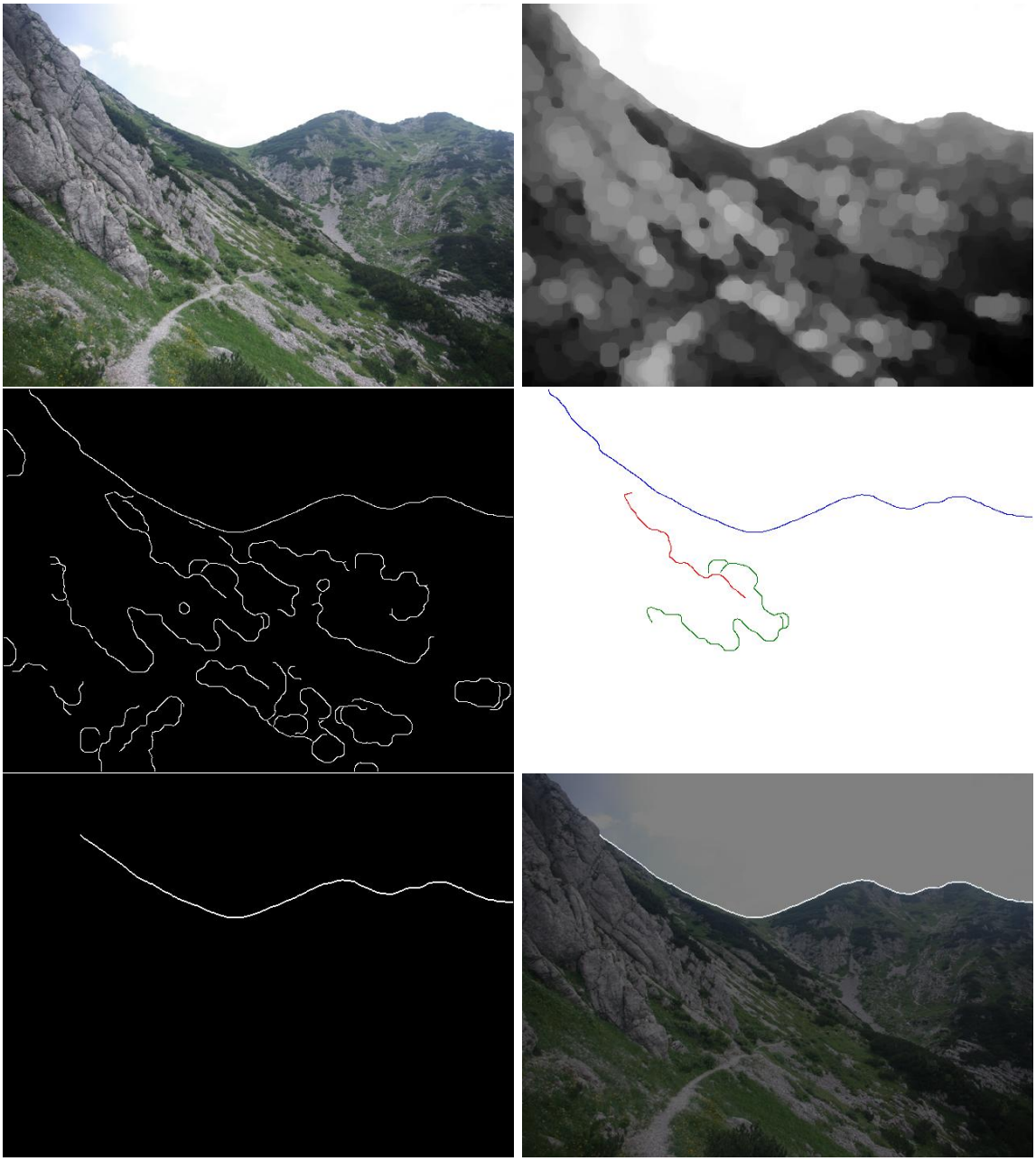

Figure A.4: Example for skyline extraction. Source: Author.

Appendix B

Circularity Indexes

Appendix B includes a detailed comparison of the different circularity measures in the examined states. The graphs illustrate the different characteristics of C_β on different districts, and the novel measure M as the area under the curve.

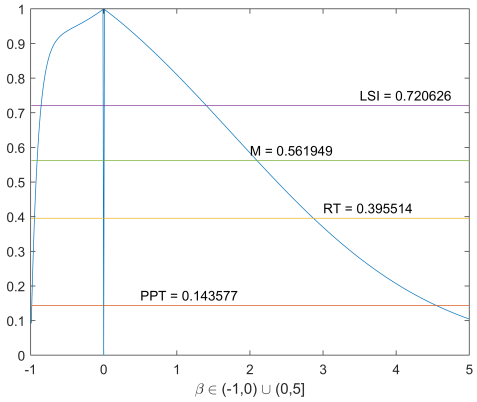

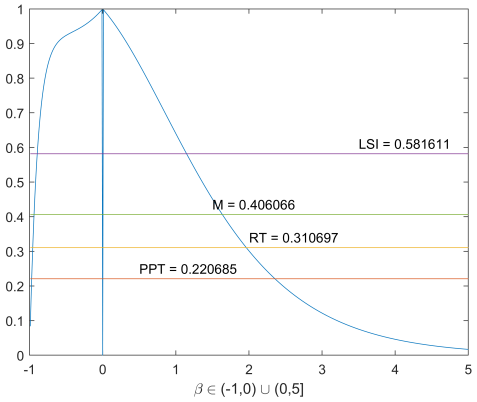

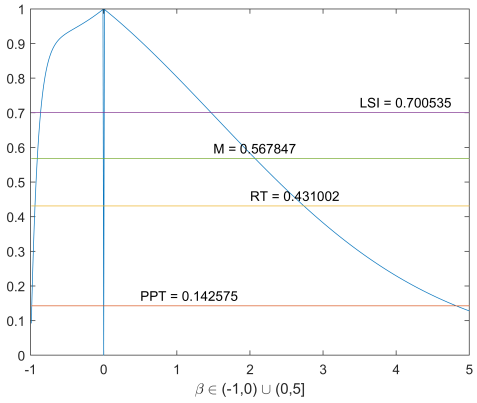

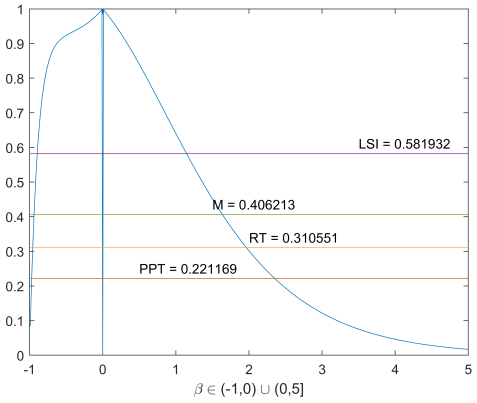

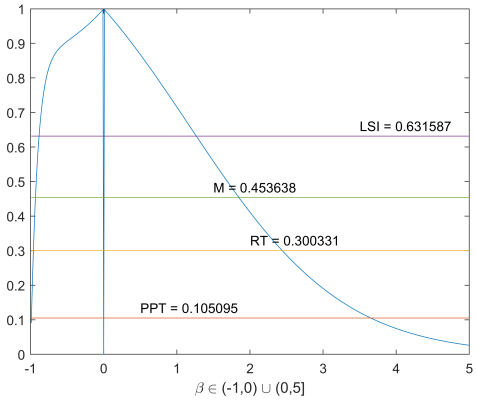

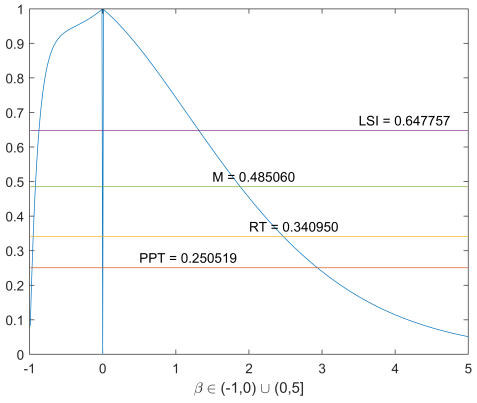

(a) The 1^{st} district.

(b) The 2^{nd} district.

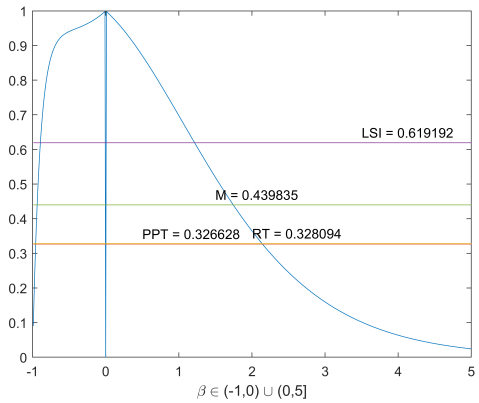

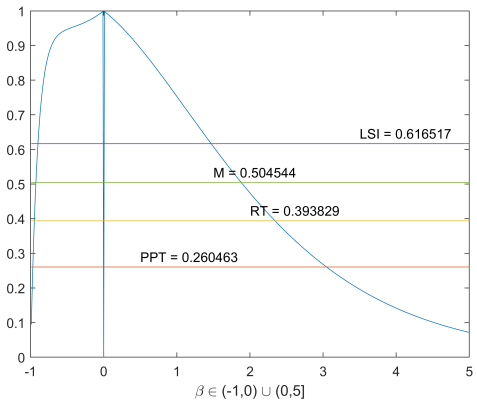

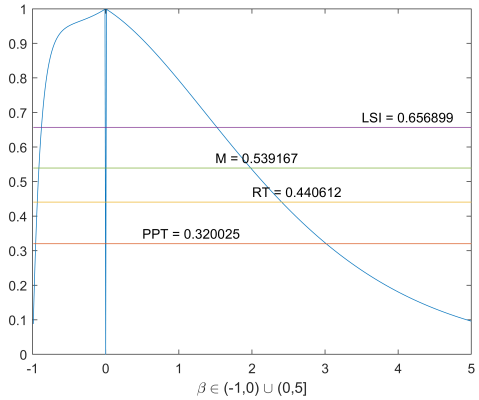

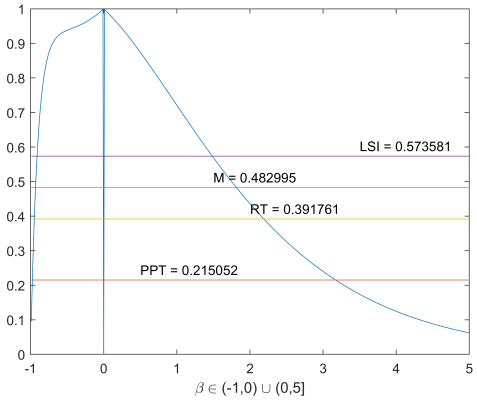

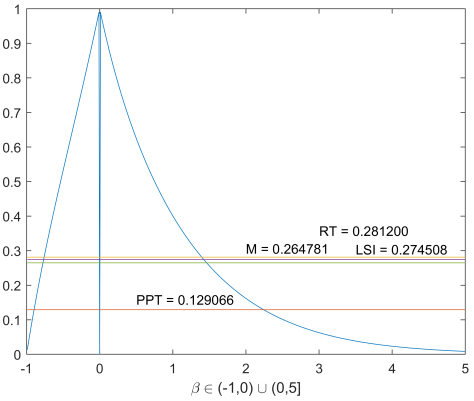

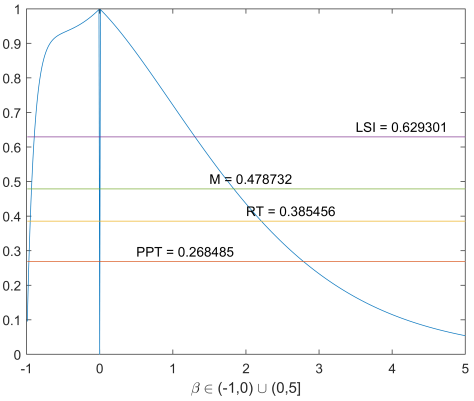

(c) The 3^{rd} district.

(d) The 4^{th} district.

Figure B.1: The circularity indexes of Arkansas for the 107^{th}, 108^{th} and the 113^{th} US Congresses from top to bottom. Source: Author.

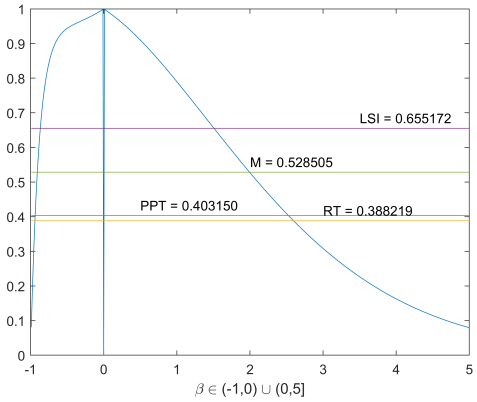

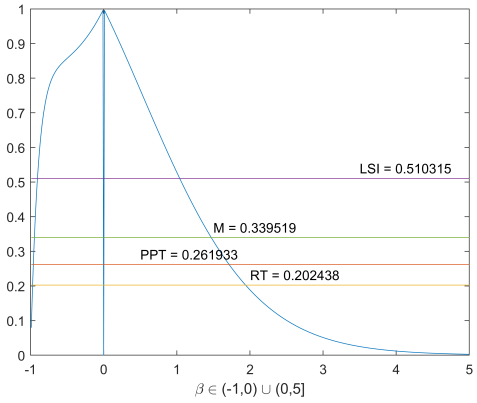

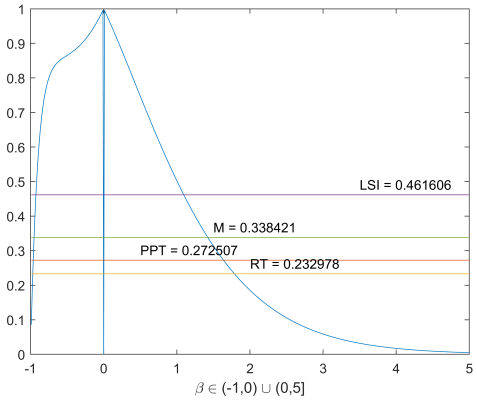

(a) The 1^{st} district.

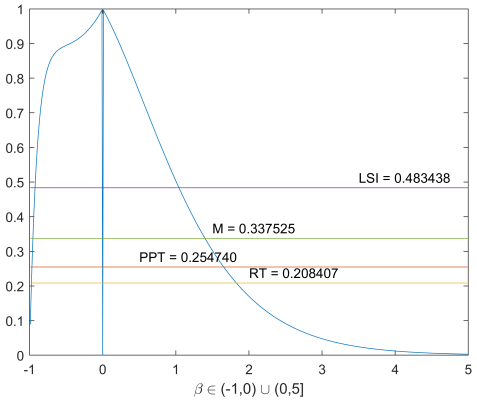

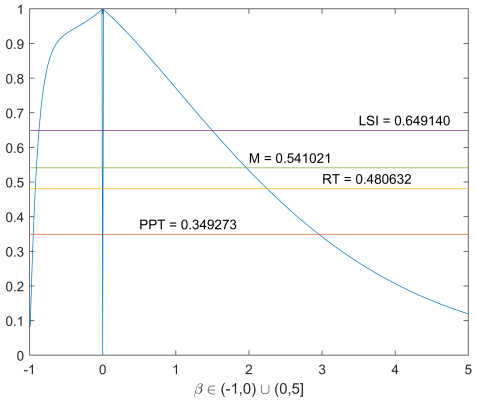

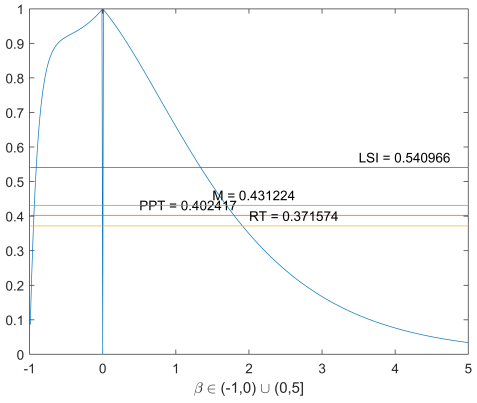

(b) The 2^{nd} district.

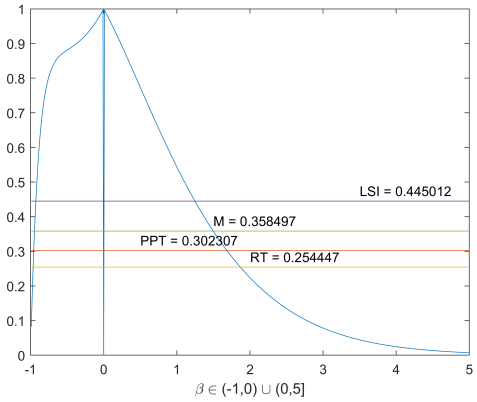

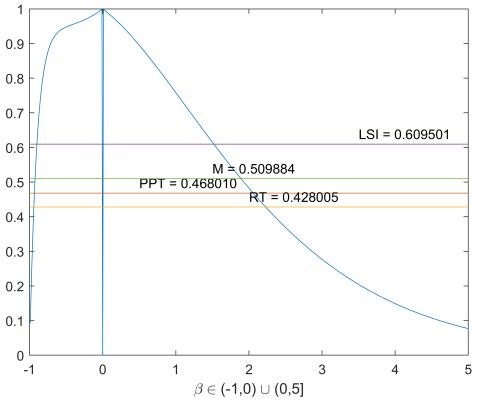

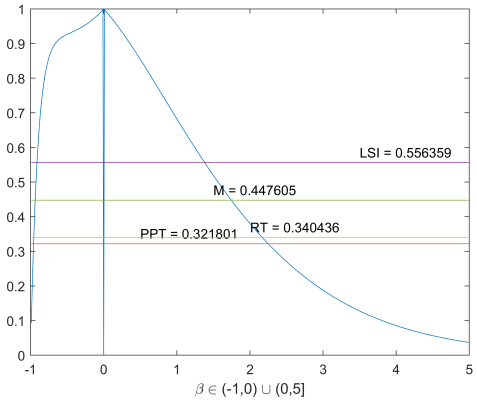

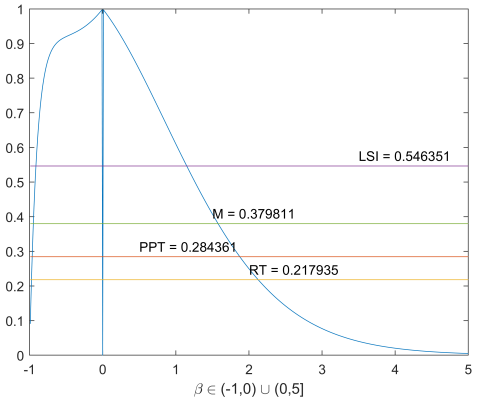

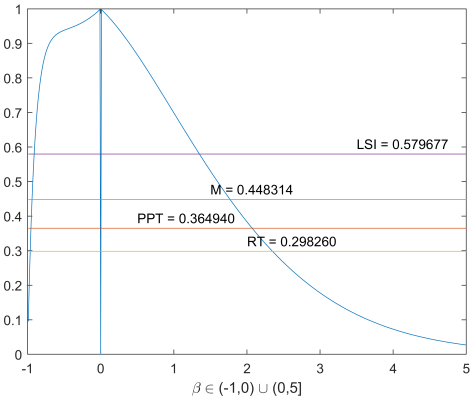

(c) The 3^{rd} district.

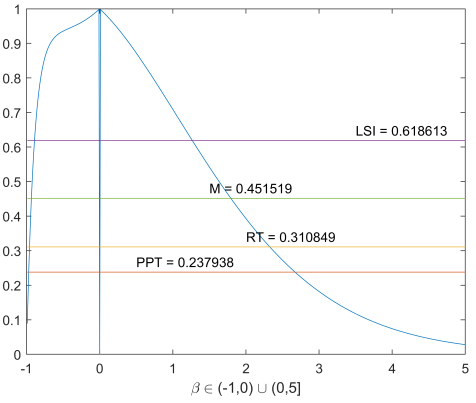

(d) The 4^{th} district.

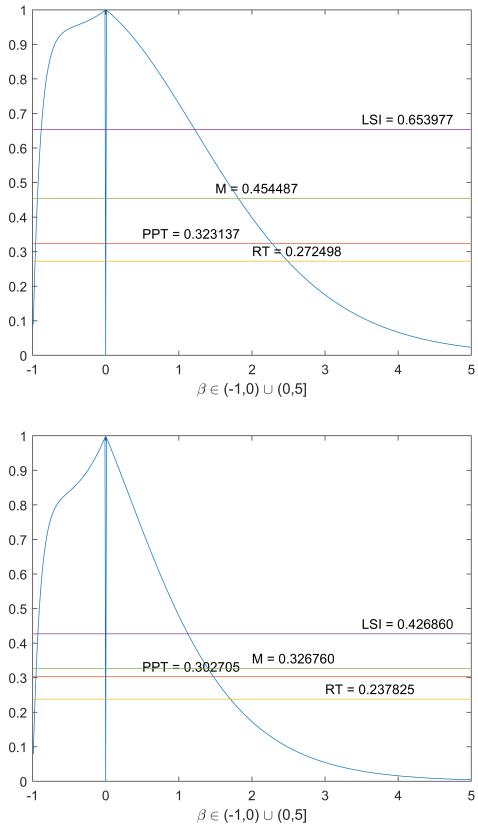

(e) The 5^{th} district, only for the 107^{th} and 108^{th}.

Figure B.2: The circularity indexes of Iowa for the 107^{th}, 108^{th} and the 113^{th} US Congresses from top to bottom. Source: Author.

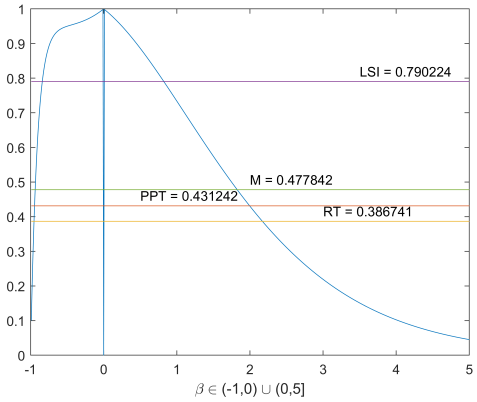

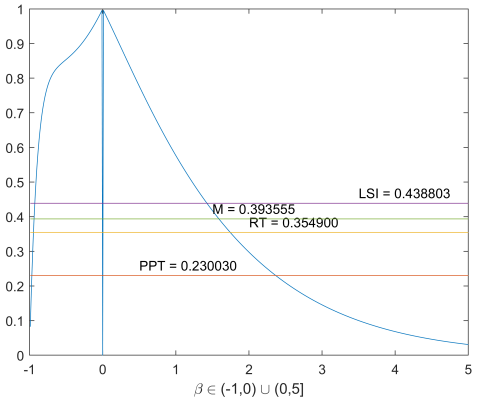

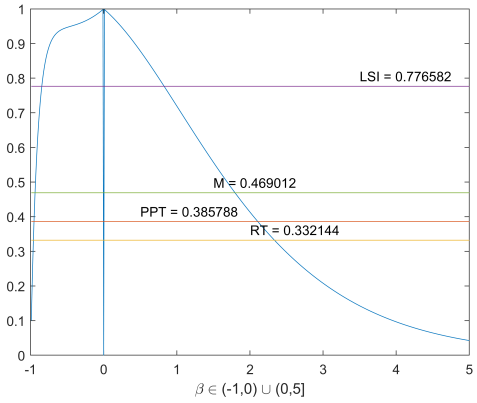

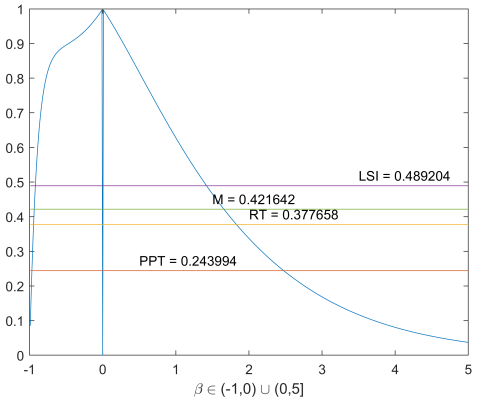

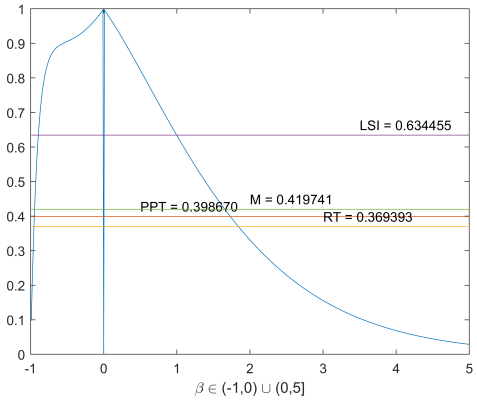

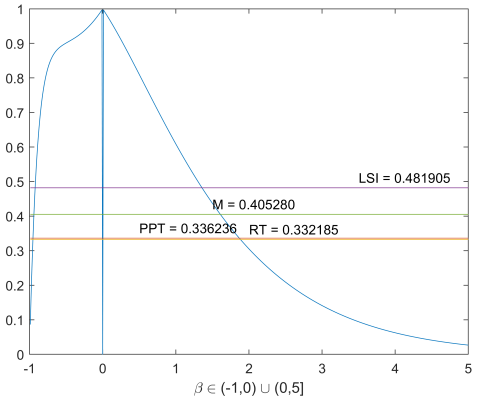

(a) The 1^{st} district.

(b) The 2^{nd} district.

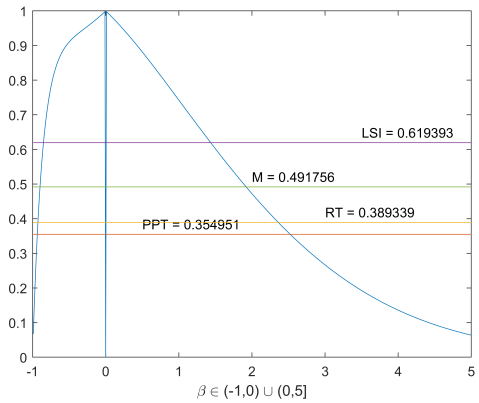

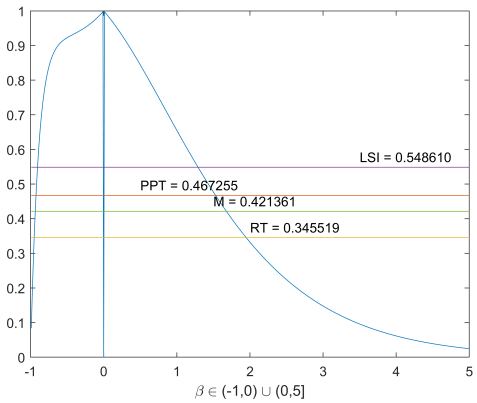

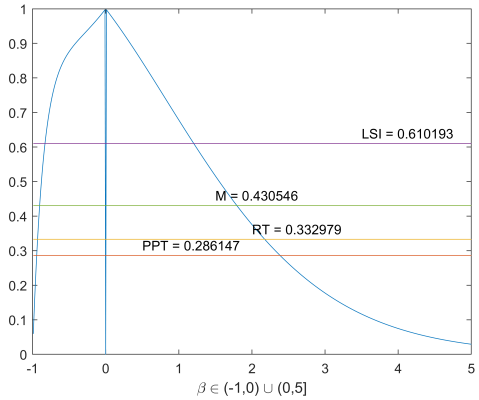

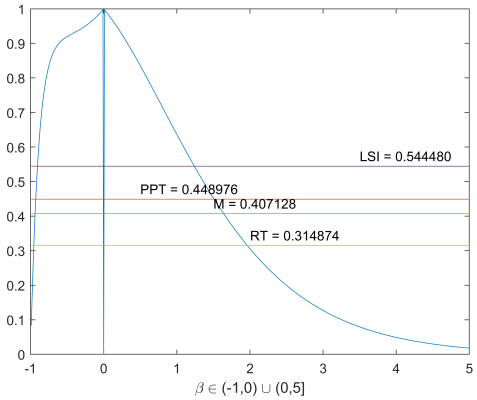

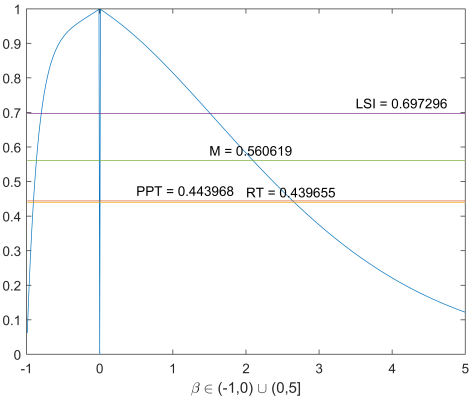

(c) The 3^{rd} district.

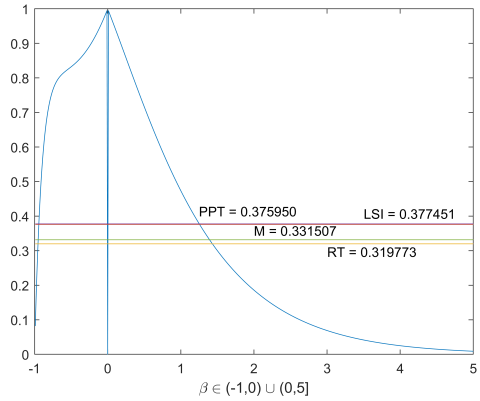

(d) The 4^{th} district.

Figure B.3: The circularity indexes of Kansas for the 107^{th}, 108^{th} and the 113^{th} US Congresses from top to bottom. Source: Author.

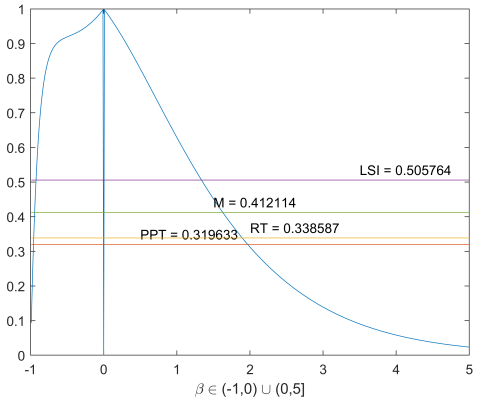

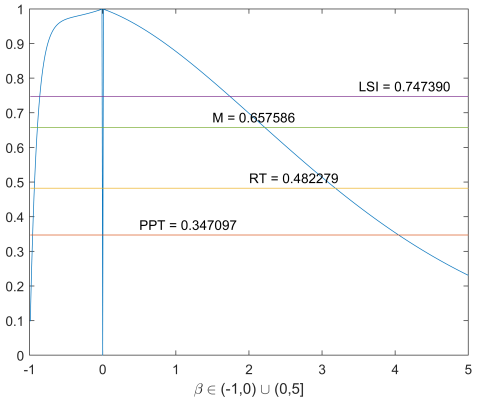

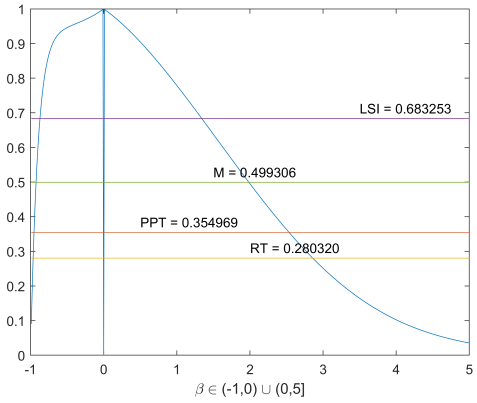

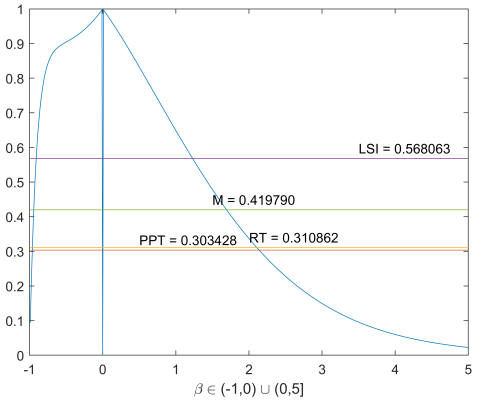

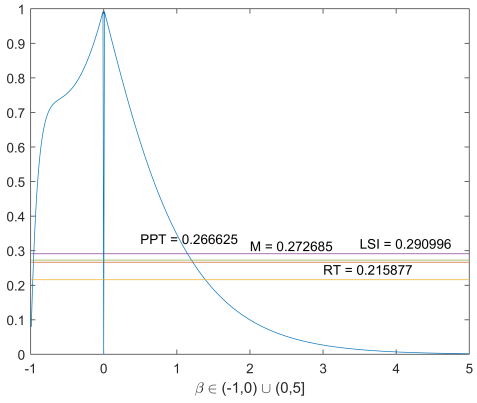

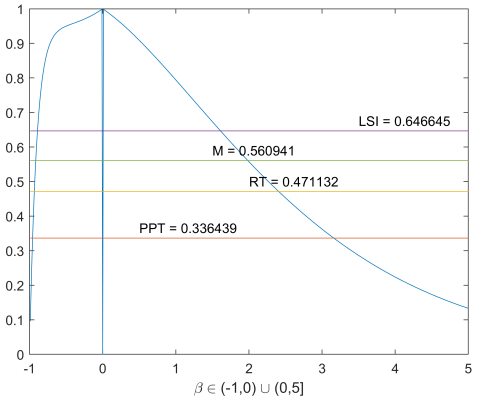

(a) The 1^{st} district.

(b) The 2^{nd} district.

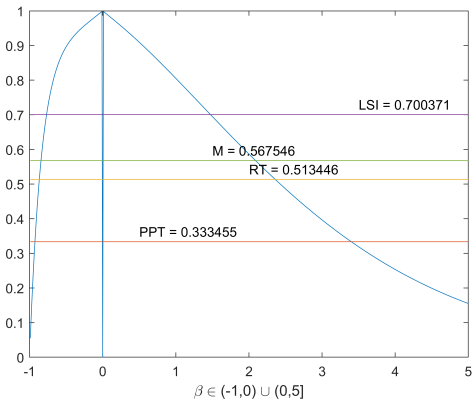

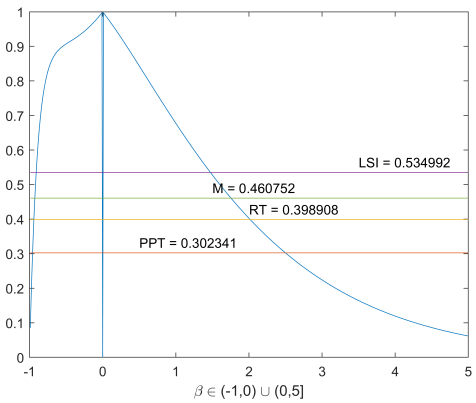

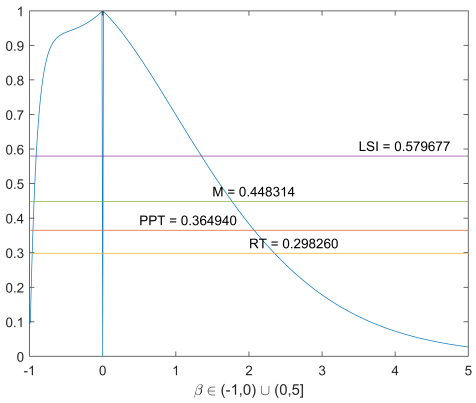

(c) The 3^{rd} district.

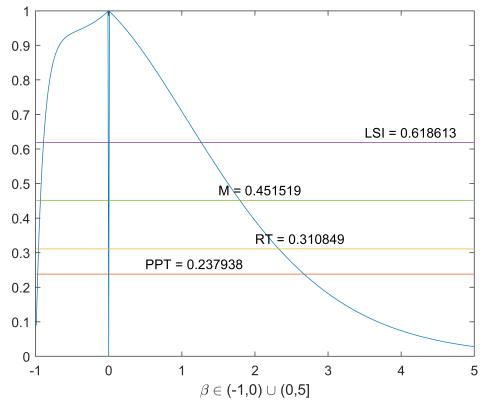

(d) The 4^{th} district, only for the 113^{th}.

Figure B.4: The circularity indexes of Utah for the 107^{th}, 108^{th} and the 113^{th} US Congresses from top to bottom. Source: Author.

Bibliography

[1] Touqeer Ahmad et al. "Comparison of semantic segmentation approaches for horizon/sky line detection". *Proceedings of the International Joint Conference on Neural Networks* (2017), pp. 4436–4443. DOI: https://doi.org/10.1109/IJCNN.2017.7966418.

[2] Micah Altman. "Is automation the answer: The computational complexity of automated redistricting". *Rutgers Computer and Law Technology Journal* 23 (1997), pp. 81–142.

[3] Micah Altman and Michael McDonald. "The promise and perils of computers in redistricting". *Duke Journal of Constitutional Law & Public Policy* 5 (2010), pp. 69–111.

[4] Stephen Ansolabehere and Maxwell Palmer. "A two hundred-year statistical history of the gerrymander". *Ohio State Law Journal* 77 (2016), p. 741.

[5] Lionel Baboud et al. "Automatic photo-to-terrain alignment for the annotation of mountain pictures". *Proceedings of the IEEE Computer Society Conference on Computer Vision and Pattern Recognition*. 2011, pp. 41–48. DOI: https://doi.org/10.1109/CVPR.2011.5995727.

[6] Fernando Bacao, Victor Lobo, and Marco Painho. "Applying genetic algorithms to zone design". *Soft Computing* 9 (2005), pp. 341–348.

[7] **Balázs Nagy**. "A new method of improving the azimuth in mountainous terrain by skyline matching". *PFG - Journal of Photogrammetry, Remote Sensing and Geoinformation Science* 88 (2020), pp. 121–131. DOI: https://doi.org/10.1007/s41064-020-00093-1.

[8] **Balázs Nagy** and Szilvia Szakál. *Circularity measures - Congressional districts of Arkansas, Iowa, Kansas and Utah (interactive map)*. http://www.researchmap.epizy.com/. Last Accessed July 15, 2020.

[9] **Balázs Nagy** and Szilvia Szakál. "Measuring the circularity of congressional districts". *Society and Economy* 42 (2020), pp. 298–312. DOI: https://doi.org/10.1556/204.2020.00008.

[10] **Balázs Nagy** and Szilvia Szakál. "Választókerületek alakjának vizsgálata Hu-féle invariáns momentumok alkalmazásával". *Alkalmazott Matematikai Lapok* 36 (2019), pp. 161–183.

[11] **Balázs Nagy** and Attila Tasnádi. "Bertrand-Edgeworth duopoly with a socially concerned firm". *Corvinus Economics Working Papers* 3 (2019).

[12] Reinhold Behringer. "Registration for outdoor augmented reality applications using computer vision techniques and hybrid sensors". *Proceedings IEEE Virtual Reality*. 1999, pp. 244–251. DOI: https://doi.org/10.1109/VR.1999.756958.

[13] Jeffrey R. Blum, Daniel G. Greencorn, and Jeremy R. Cooperstock. "Smartphone sensor reliability for augmented reality applications". 2013, pp. 127–138. DOI: https://doi.org/10.1007/978-3-642-40238-8_11.

[14] Burçin Bozkaya, Erhan Erkut, and Gilbert Laporte. "A tabu search heuristic and adaptive memory procedure for political districting". *European Journal of Operational Research* 144 (2003), pp. 12–26.

[15] John Canny. "A computational approach to edge detection". *IEEE Transactions on Pattern Analysis and Machine Intelligence* 8 (1986), pp. 679–698. DOI: https://doi.org/10.1109/TPAMI.1986.4767851.

[16] Christopher P. Chambers. "An axiomatic theory of political representation". *Journal of Economic Theory* 144 (2009), pp. 375–389. DOI: https://doi.org/10.1016/j.jet.2008.06.005.

[17] Christopher P. Chambers and Alan D. Miller. "A measure of bizarreness". *Quarterly Journal of Political Science* 5 (2010), pp. 27–44. DOI: https://doi.org/10.1561/100.00009022.

[18] Christopher P. Chambers and Alan D. Miller. "Measuring legislative boundaries". *Mathematical Social Sciences* 66 (2013), pp. 268–275. DOI: https://doi.org/10.1016/j.mathsocsci.2013.06.001.

[19] Chung-I Chou and Sai-Ping Li. "Taming the gerrymander—statistical physics approach to political districting problem". *Physica A: Statistical Mechanics and its Applications* 369 (2006), pp. 799–808.

[20] Dimitrij Csetverikov. *Digitális képelemzés alapvető algoritmusai*. Eötvös Loránd Tudományegyetem, Informatikai Kar, 2014.

[21] Tamás Dusek. "A megyék és régiók összehasonlítása alakmutatókkal". *Területi Statisztika* 55 (2015), pp. 142–156.

[22] Chao Fan et al. "A spatiotemporal compactness pattern analysis of congressional districts to assess partisan gerrymandering: A case study with California and North Carolina". *Annals of the Association of American Geographers* 105 (2015), pp. 736–753. DOI: https://doi.org/10.1080/00045608.2015.1039109.

[23] Tom G. Farr et al. "The Shuttle Radar Topography Mission". *Reviews of Geophysics* 45 (2007). DOI: https://doi.org/10.1029/2005RG000183.

[24] Roman Fedorov, Darian Frajberg, and Piero Fraternali. "A framework for outdoor mobile augmented reality and its application to mountain peak detection". *Augmented Reality, Virtual Reality, and Computer Graphics*. Ed. by Lucio Tommaso De Paolis and Antonio Mongelli. Springer International Publishing, 2016, pp. 281–301. DOI: https://doi.org/10.1007/978-3-319-40621-3_21.

[25] Roman Fedorov, Piero Fraternali, and Marco Tagliasacchi. "Mountain peak identification in visual content based on coarse digital elevation models". *Proceedings of the 3rd ACM International Workshop on Multimedia Analysis for Ecological Data*. 2014, pp. 7–11. DOI: https://doi.org/10.1145/2661821.2661825.

[26] Balázs Fleiner, **Balázs Nagy**, and Attila Tasnádi. "Optimal partisan districting on planar geographies". *Central European Journal of Operations Research* 25 (2017), pp. 879–888. DOI: https://doi.org/10.1007/s10100-016-0454-7.

[27] Michael R. Garey and David S. Johnson. W. H. Freeman and Company, 1979.

[28] Robert S. Garfinkel and George L. Nemhauser. "Optimal political districting by implicit enumeration techniques". *Management Science* 16 (1970), B495–B508. URL: http://www.jstor.org/stable/2628656.

[29] Lifeng He et al. "The connected-component labeling problem: A review of state-of-the-art algorithms". *Pattern Recognition* 70 (2017), pp. 25–43. DOI: https://doi.org/10.1016/j.patcog.2017.04.018.

[30] Sidney Wayne Hess et al. "Nonpartisan political redistricting by computer". *Operations Research* 13 (1965), pp. 998–1006. DOI: https://doi.org/10.1287/opre.13.6.998.

[31] Michael Hölzl, Roland Neumeier, and Gerald Ostermayer. "Analysis of Compass Sensor Accuracy on Several Mobile Devices in an Industrial Environment". *Computer Aided Systems Theory - EUROCAST 2013*. 2013, pp. 381–389. DOI: https://doi.org/10.1007/978-3-642-53862-9_49.

[32] Ming-Kuei Hu. "Visual pattern recognition by moment invariants". *IRE Transactions on Information Theory* 8 (1962), pp. 179–187. DOI: https://doi.org/10.1109/TIT.1962.1057692.

[33] Yao-Ling Hung et al. "Skyline localization for mountain images". *2013 IEEE International Conference on Multimedia and Expo (ICME)*. 2013, pp. 1–6.

[34] Iwan Jensen. "Counting polyominoes: A parallel implementation for cluster computing". *International Conference on Computational Science*. 2003, pp. 203–212.

[35] Jörg Kalcsics. "Districting Problems". *Location Science*. Springer, 2015, pp. 595–622. DOI: https://doi.org/10.1007/978-3-319-13111-5_23.

[36] Stephan Karpischek et al. "SwissPeaks - Mobile augmented reality to identify mountains". *Proceedings of the 3rd European Conference on Ambient Intelligente*. 2009.

[37] László Kóczy, Péter Biró, and Balázs Sziklai. "Fair apportionment in the view of the Venice Commission's recommendation". *Mathematical Social Sciences* 77 (2015), pp. 32–41. DOI: https://doi.org/10.1016/j.mathsocsci.2015.06.001.

[38] László Kóczy, Péter Biró, and Balázs Sziklai. "US vs. European apportionment practices: The conflict between monotonicity and proportionality". *Trends in Computational Social Choice* (2017), pp. 309–325.

[39] David R. Lee and G. Thomas Sallee. "A method of measuring shape". *Geographical Review* 60 (1970), pp. 555–563. DOI: https://doi.org/10.2307/213774.

[40] Justin Levitt. *All about redistricting*. http://redistricting.lls.edu/. Last Accessed January 24, 2019.

[41] Yoad Lewenberg, Omer Lev, and Jeffrey S. Rosenschein. "Divide and conquer: Using geographic manipulation to win district-based elections". *Proceedings of the 16th Conference on Autonomous Agents and MultiAgent Systems*. International Foundation for Autonomous Agents and Multiagent Systems. 2017, pp. 624–632.

[42] Wen-Nung Lie et al. "A robust dynamic programming algorithm to extract skyline in images for navigation". *Pattern Recognition Letters* 26 (2005), pp. 221–230. DOI: https://doi.org/10.1016/j.patrec.2004.08.021.

[43] Brian J. Lunday. "A metric to identify gerrymandering". *International Journal of Society Systems Science* 6 (2014), pp. 285–304. DOI: https://doi.org/10.1504/ijsss.2014.065207.

[44] Mona Lütjens et al. "Virtual reality in cartography: Immersive 3D visualization of the Arctic Clyde Inlet (Canada) using digital elevation models and bathymetric data". *Multimodal Technologies and Interaction* 3 (2019), p. 9. DOI: https://doi.org/10.3390/mti3010009.

[45] Alan M. Maceachren. "Compactness of geographic shape: Comparison and evaluation of measures". *Geografiska Annaler. Series B, Human Geography* 67 (1985), pp. 53–67. DOI: https://doi.org/10.1080/04353684.1985.11879515.

[46] Anuj Mehrotra, Ellis L. Johnson, and George L. Nemhauser. "An optimization based heuristic for political districting". *Management Science* 44 (1998), pp. 1100–1114. URL: http://www.jstor.org/stable/2634689.

[47] Stuart S. Nagel. "Computers & the law & politics of redistricting". *Polity* 5 (1972), pp. 77–93. DOI: https://doi.org/10.2307/3234042.

[48] NASA/METI/AIST/Japan Spacesystems, and U.S./Japan ASTER Science Team. "ASTER Global Digital Elevation Model". *NASA EOSDIS Land Processes DAAC* (2009). DOI: https://doi.org/10.5067/ASTER/ASTGTM.002.

[49] Prospero C. Naval et al. "Estimating camera position and orientation from geographical map and mountain image". *38th Research Meeting of the Pattern Sensing Group, Society of Instrument and Control Engineers*. 1997, pp. 9–16.

[50] Amiya Nayak and Ivan Stojmenovic. Wiley-IEEE. Wiley, 2007, pp. 347–372.

[51] Richard G. Niemi et al. "Measuring compactness and the role of a compactness standard in a test for partisan and racial gerrymandering". *The Journal of Politics* 52 (1990), pp. 1155–1181.

[52] Johannes Oehrlein and Jan-Henrik Haunert. "A cutting-plane method for contiguity-constrained spatial aggregation". *Journal of Spatial Information Science* 15 (2017), pp. 89–120. DOI: https://doi.org/10.5311/josis.2017.15.379.

[53] Politecnico di Milano. *PeakLens*. https://peaklens.com. Last Accessed August 13, 2019.

[54] Daniel D. Polsby and Robert D. Popper. "The third criterion: Compactness as a procedural safeguard against partisan gerrymandering". *Yale Law & Policy Review* 9 (1991), pp. 301–353.

[55] Clemens Puppe and Attila Tasnádi. "Axiomatic districting". *Social Choice and Welfare* 44 (2015), pp. 31–50. DOI: https://doi.org/10.1007/s00355-014-0824-9.

[56] Clemens Puppe and Attila Tasnádi. "Optimal redistricting under geographical constraints: Why "pack and crack" does not work". *Economics Letters* 105 (2009), pp. 93–96. DOI: https://doi.org/10.1016/j.econlet.2009.06.008.

[57] Srikumar Ramalingam et al. "SKYLINE2GPS: Localization in urban canyons using omni-skylines". *2010 IEEE/RSJ International Conference on Intelligent Robots and Systems, IROS 2010 - Conference Proceedings*. 2010, pp. 3816–3823. DOI: https://doi.org/10.1109/IROS.2010.5649105.

[58] Ernest C. Reock. "A note: Measuring compactness as a requirement of legislative apportionment". *Midwest Journal of Political Science* 5 (1961), pp. 70–74. DOI: https://doi.org/10.2307/2109043.

[59] Federica Ricca, Andrea Scozzari, and Bruno Simeone. "Political districting: From classical models to recent approaches". *4OR* 9 (2011), p. 223. DOI: https://doi.org/10.1007/s10288-011-0177-5.

[60] Federica Ricca, Andrea Scozzari, and Bruno Simeone. "Weighted Voronoi region algorithms for political districting". *Mathematical and Computer Modelling* 48 (2008), pp. 1468–1477. DOI: https://doi.org/10.1016/j.mcm.2008.05.041.

[61] Federica Ricca and Bruno Simeone. "Local search algorithms for political districting". *European Journal of Operational Research* 189 (2008), pp. 1409–1426. DOI: https://doi.org/10.1016/j.ejor.2006.08.065.

[62] Routes Software SRL. *PeakVisor*. https://peakvisor.com. Last Accessed August 6, 2019.

[63] Antonio La Salandra, Darian Frajberg, and Piero Fraternali. "A virtual reality application for augmented panoramic mountain images". *Virtual Reality* (2019). DOI: https://doi.org/10.1007/s10055-019-00385-x.

[64] Olivier Saurer et al. "Image-based large-scale geo-localization in mountainous regions". *Advances in Computer Vision and Pattern Recognition* (2016), pp. 205–223. DOI: https://doi.org/10.1007/978-3-319-25781-5_11.

[65] Fabio Soldati. *PeakFinder AR*. https://peakfinder.ch. Last Accessed August 6, 2019.

[66] Fridtjor Stein and Gerard Medioni. "Map-based localization using the panoramic horizon". *IEEE Transactions on Robotics and Automation* 11 (1995), pp. 892–896. DOI: https://doi.org/10.1109/70.478436.

[67] Richard Szeliski. *Computer Vision - Algorithms and Applications*. Texts in Computer Science. 2011. DOI: https://doi.org/10.1007/978-1-84882-935-0.

[68] Balázs R. Sziklai and Károly Héberger. "Apportionment and districting by Sum of Ranking Differences". *PLOS ONE* 15 (Mar. 2020), pp. 1–20. DOI: https://doi.org/10.1371/journal.pone.0229209.

[69] Attila Tasnádi. "The political districting problem: A survey". *Society and Economy* 33 (2011), pp. 543–554. DOI: https://doi.org/10.1556/SocEc.2011.0001.

[70] Eric Tzeng et al. "User-driven geolocation of untagged desert imagery using digital elevation models". *2013 IEEE Computer Society Conference on Computer Vision and Pattern Recognition Workshops*. 2013, pp. 237–244. DOI: https://doi.org/10.1109/CVPRW.2013.42.

[71] US Census Bureau. *Cartographic boundary shapefiles - Congressional districts*. https://www.census.gov/geo/maps-data/. Last Accessed January 17, 2019.

[72] William Vickrey. "On the prevention of gerrymandering". *Political Science Quarterly* 76 (1961), pp. 105–110. DOI: https://doi.org/10.2307/2145973.

[73] Gerald R. Webster. "Reflections on current criteria to evaluate redistricting plans". *Political Geography* 32 (2013), pp. 3–14. DOI: https://doi.org/10.1016/j.polgeo.2012.10.004.

[74] Jihwan Woo et al. "Vision-based UAV navigation in mountain area". *Proceedings of the IAPR Conference on Machine Vision Applications 2007), May 16-18, 2007, Tokyo, Japan.* Vol. 1. 2007, pp. 3–6.

[75] H. Peyton Young. "Measuring the compactness of legislative districts". *Legislative Studies Quarterly* 13 (1988), pp. 105–115.

[76] Shupeng Zhu et al. "Skyline matching: A robust registration method between Video and GIS". *Usage, Usability, and Utility of 3D City Models.* 2012, p. 7. DOI: https://doi.org/10.1051/3u3d/201203007.

[77] Joviša Žunić. "Shape descriptors for image analysis". *Zbornik Radova MI-SANU* 15 (2012), pp. 5–38.

[78] Joviša Žunić, Kaoru Hirota, and Paul L. Rosin. "A Hu moment invariant as a shape circularity measure". *Pattern Recognition* 43 (2010), pp. 47–57. DOI: https://doi.org/10.1016/j.patcog.2009.06.017.